Computational Study of the Reactions of Methanol with the Hydroperoxyl and Methyl Radicals. 1. Accurate Thermochemistry and Barrier Heights

ARTICLE *in* THE JOURNAL OF PHYSICAL CHEMISTRY A · MARCH 2011

Impact Factor: 2.69 · DOI: 10.1021/jp110024e · Source: PubMed

2 AUTHORS, INCLUDING:

Donald Truhlar
University of Minnesota Twin Cities
1,342 PUBLICATIONS **81,184** CITATIONS

SEE PROFILE

THE JOURNAL OF PHYSICAL CHEMISTRY A

ARTICLE

pubs.acs.org/JPCA

Computational Study of the Reactions of Methanol with the Hydroperoxyl and Methyl Radicals. 1. Accurate Thermochemistry and Barrier Heights

I. M. Alecu and Donald G. Truhlar*

Department of Chemistry and Supercomputing Institute, University of Minnesota, Minneapolis, Minnesota 55455-0431, United States

Supporting Information

ABSTRACT: The reactions of CH_3OH with the HO_2 and CH_3 radicals are important in the combustion of methanol and are prototypes for reactions of heavier alcohols in biofuels. The reaction energies and barrier heights for these reaction systems are computed with CCSD(T) theory extrapolated to the complete basis set limit using correlation-consistent basis sets, both augmented and unaugmented, and further refined by including a fully coupled treatment of the connected triple excitations, a second-order perturbative treatment of quadruple excitations (by $CCSDT(2)_Q$), core−valence corrections, and scalar relativistic effects. It is shown that the M08-HX and M08-SO hybrid meta-GGA density functionals can achieve sub-kcal mol^{-1} agreement with the high-level ab initio results, identifying these functionals as important potential candidates for direct dynamics studies on the rates of these and homologous reaction systems.

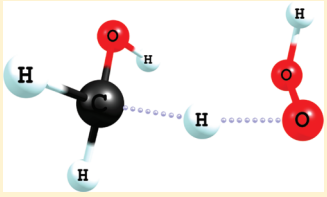

1. INTRODUCTION

One important aim of modern combustion chemistry is to design and analyze possible new forms of nonpetroleum-based fuel or fuel components for use in combustion engines. Ethanol is an example of such a fuel source, and its success as an additive to conventional gasoline fuel has generated interest in the investigation of other similar compounds as possible alternative fuels. One such compound is 1-butanol, a promising biofuel that will soon be commercially available for use as a gasoline-blending component in combustion engines.

In the combustion of heavy alcohols, dehydrogenation and dehydration reactions can respectively generate many oxygenated and nonoxygenated intermediates directly from the fuel. Many of the reagents and transition states are cyclic or have many torsions, so that the reaction system is complex, and a systematic approach must be devised in order to arrive at reliable conclusions about the overall mechanism. In the present article, our goal is to explore the reactions of the simplest alcohol, methanol, as a first step toward characterizing larger and more difficult systems.

Under a wide range of experimental conditions, the methanol oxidation pathway involves successive dehydrogenations;[1] only trace amounts of methane or other hydrocarbons (products of dehydration reactions) are observed in the combustion of methanol since this simple alcohol does not possess β C−H bonds—the cleavage of which is the important step which precedes the β-scission of the OH group in the dehydration of heavier alcohols.[1,2] Dehydrogenation by abstraction of H-atoms from the alcohol can be accomplished by various radicals produced during combustion, such as the hydroperoxyl radical, the reactions of which have been shown[3] to drive much of the chemistry involved in the combustion of methanol, and the methyl radical, which is readily produced during the oxidation and pyrolysis of methanol.[3,4] In this study, we consider all four of the possible hydrogen abstraction reactions of hydroperoxyl radical and methyl radical with methanol:

$$CH_3OH + HO_2 \rightarrow CH_2OH + HOOH \quad (R1a)$$

$$CH_3OH + HO_2 \rightarrow CH_3O + HOOH \quad (R1b)$$

$$CH_3OH + CH_3 \rightarrow CH_2OH + CH_4 \quad (R2a)$$

$$CH_3OH + CH_3 \rightarrow CH_3O + CH_4 \quad (R2b)$$

Two recent studies focusing on the overall mechanism of methanol combustion have indicated that this mechanism is highly sensitive to the rates of reactions R1a and R1b.[5,6] However, the above reactions have received little experimental attention in the literature due to the fact that the HO_2 and CH_3 radicals are challenging to study experimentally. There is also the theoretical question of whether HO_2 has too much multireference character to be adequately treated by single-reference methods. The CH_3O and CH_2OH radicals produced in these reactions have been implicated in important processes[7,8] in the fields of astrophysics, environmental chemistry, and combustion chemistry, and they are also problematic as the former exhibits significant Jahn−Teller distortion and spin−orbit coupling while the latter is a highly nonrigid molecule with several vibrational modes characterized by appreciable anharmonicity.[9−13]

The purpose of this article is threefold. First, we provide accurate benchmark results for the bond energies, reaction

Received: October 19, 2010
Revised: February 10, 2011
Published: March 15, 2011

energies, and barrier heights of these four reactions. Second, we investigate how well high-level single-reference approaches, based on coupled cluster theory but short of benchmark quality, can characterize the thermochemistry and barrier heights of these complex reaction systems. This is important because we are ultimately interested in characterizing larger but analogous systems. Finally, we seek to establish a more affordable electronic model chemistry, based on density functional approximations, that can be used in future direct dynamics calculations without significantly compromising the accuracy.

2. GENERAL OVERVIEW OF METHODOLOGY

In section 2.1, we compile databases of accurate experimental bond dissociation enthalpies and heats of reaction for the reaction systems presently investigated. Furthermore, we supplement the thermochemical quantities in these databases with their zero-point-exclusive counterparts by subtracting the contributions from vibrational zero-point energies (ZPEs) taken from experiments, given by high-level computations, or accurately estimated in this work. These data will serve as the most accurate experimentally derived quantities to which the computed analogues can be compared.

The next step in understanding these reactions is to find an accurate quantum mechanical computational method that can characterize the thermochemistry of these reaction systems successfully and predict reliable barrier heights. Section 2.2 will describe several single-reference electronic structure levels, some based on wave function theory (WFT) and others on density functional theory (DFT); the wave function levels and density functionals will be combined with one-electron basis sets to define model chemistries[14] that can be used to explore the thermochemistry of the methanol combustion reactions.

2.1. Databases of Accurate Bond Energies and Reaction Energies. For a direct comparison to experimental quantities such as bond dissociation enthalpies and enthalpies of reaction at 0 K, D_0 and ΔH_0°, respectively, it is necessary to compute the electronic (Born−Oppenheimer) energies and the zero-point energies (ZPE) of the species in question. However, the accuracy of electronic model chemistries may be masked by the addition of computed ZPEs, which can be less accurate. Therefore, the true accuracy of a given electronic model chemistry can be better gauged by comparing zero-point-exclusive quantities, and in this section, we are interested in establishing and comparing zero-point-exclusive bond energies and reaction energies, D_e and ΔE, respectively.

First we consider $D_e(H-OCH_3)$, $D_e(H-CH_2OH)$, $D_e(H-OOH)$, and $D_e(H-CH_3)$, since these quantities can be combined as shown in eq 1 to yield ΔE values for any of the methanol reactions above.

$$\Delta E = D_e(H-X) - D_e(H-Y) \quad (1)$$

In eq 1, X represents the fragment from which the H-atom is being transferred, and Y is the fragment to which the H-atom is being transferred (i.e., X is the donor and Y is the acceptor). It is straightforward to obtain D_e values from computations, but to obtain D_e values from experiments, one must remove ZPEs from the experimental quantities of interest:

$$D_e(H-X) = D_0(H-X) - ZPE(X) + ZPE(HX) \quad (2)$$

$$\Delta E = \Delta H_0^\circ - \Delta ZPE \quad (3)$$

$$\Delta H_0^\circ = D_0(H-X) - D_0(H-Y) \quad (4)$$

$$\Delta ZPE = ZPE(HY) + ZPE(X) - ZPE(HX) - ZPE(Y) \quad (5)$$

Strictly speaking, the ZPE is not an experimental quantity (i.e., it cannot be measured spectroscopically or by a thermochemical process since there are no stationary states at energies lower than the ground state); however, it can be *estimated* from spectroscopic data obtained from experiments. Fewer spectroscopic parameters are required to estimate the ZPEs of diatomic molecules than those of polyatomic species; consequently, the "experimental" ZPEs for many diatomics are readily available while only a few have been estimated for stable polyatomic molecules, and even fewer for molecular free radicals.

Recently, we proposed an alternative method for reasonably estimating the ZPE of a typical molecule or molecular radical by using universal scale factor ratios.[15] The ratio $\alpha^{F/ZPE}$ between scale factors optimized for fundamental frequencies (F) and ZPEs, respectively, was found to be almost constant for 40 electronic model chemistries we tested, leading to the recommendation of the average value of 0.974 as a "universal" scale factor ratio. Thus, we proposed that for a molecule or molecular radical characterized by covalent bonds, the equation

$$\varepsilon_{vib}^{G} \cong \frac{hc}{2\alpha^{F/ZPE}} \sum_m \upsilon_m \quad (6)$$

where h is Planck's constant and c is the speed of light, can be used to approximate the ZPE, ε_{vib}^{G}, by summing over all of its observed fundamental vibrational frequencies, υ_m. We explored the accuracy of the ZPEs predicted via eq 6 by comparing these predictions to a database of 18 accurate experimental ZPEs, and we determined 2σ uncertainty of $\pm 1.6\%$ for ZPEs estimated by this equation.[15]

Therefore, our approach for compiling databases of accurate zero-point-exclusive bond energies and reaction energies is as follows: (i) obtain D_0 values in the usual way by combining accurate experimental heats of formation ($\Delta_f H_0^\circ$), (ii) obtain ZPE values for all species from the literature or via eq 6, and (iii) use eqs 2−5 to combine the quantities from steps i and ii to obtain accurate estimates for the quantities of interest. With the exceptions of CH_3O and CH_2OH, following the three-step procedure described above is fairly straightforward: we take the heats of formation and corresponding 2σ confidence limits from the recent critical evaluations of Ruscic et al.[16−18] and we obtain the ZPEs via eq 6 (with the allowance of 1.6% error margins as 2σ), where the observed vibrational fundamental frequencies are taken from the Computational Chemistry Comparison and Benchmark Database.[19]

The accurate assessment of the thermochemistry of CH_3O requires the use of a molecular Hamiltonian that accounts for the spin-vibronic effects brought about by the Jahn−Teller distortion and spin−orbit coupling exhibited by the ground ^2E electronic state of CH_3O. Recently, Marenich and Boggs implemented a spin-vibronic Hamiltonian that also accounted for anharmonic effects to compute the thermochemistry of the CH_3O system from accurate partition functions calculated from the explicit summation of Boltzmann factors based on the eigenenergies.[10] In addition, in the same work, Marenich and Boggs carefully arrived at a reliable estimate for $\Delta_f H_0^\circ(CH_3O)$ by studying the enthalpies of four reactions involving the CH_3O radical, using electronic energies computed from high-level coupled cluster calculations extrapolated to the complete basis

Table 1. Experimental Enthalpies of Formation and Zero-Point Energies (kcal mol^{-1}) for Reactants and Products of Methanol Reactions

property	H	HO_2	HOOH	CH_3OH	CH_2OH	CH_3O	CH_3	CH_4
$\Delta_f H_0^{\circ a}$	51.63337 ± 0.00002	3.64 ± 0.06	−31.01 ± 0.04	−45.44 ± 0.14	−2.53 ± 0.17	7.36 ± 0.22	35.85 ± 0.07	−15.92 ± 0.07
ZPE^b	0.00	8.70 ± 0.14	16.33 ± 0.26	31.85 ± 0.51	22.59 ± 0.02	22.60 ± N/A	18.68 ± 0.30	27.83 ± 0.45

[a] $\Delta_f H_0^\circ$ values for CH_3O taken from ref 10; $\Delta_f H_0^\circ$ value for CH_2OH taken from ref 13; $\Delta_f H_0^\circ$ value for H taken from ref 16; $\Delta_f H_0^\circ$ values for HOOH, CH_3OH, CH_3, and CH_4 taken from ref 17; $\Delta_f H_0^\circ$ value for HO_2 taken from ref 18. [b] ZPE for CH_3O taken from ref 10; ZPE for CH_2OH taken from ref 13; ZPEs for HO_2, HOOH, CH_3OH, CH_3, and CH_4 estimated via eq 6 from text.

Table 2. Experimental R−H Bond Energies (kcal mol^{-1}) for HOOH, CH_3OH, and CH_4

property	H−OOH	H−CH_2OH	H−OCH_3	H−CH_3
D_0^a	86.28 ± 0.07	94.54 ± 0.22	104.43 ± 0.26	103.41 ± 0.10
D_e^b	93.91 ± 0.30	103.80 ± 0.56	112.91 ± 0.57	112.56 ± 0.55

[a] D_0 values were derived using the $\Delta_f H_0^\circ$ values from Table 1. [b] D_e values were derived using the $\Delta_f H_0^\circ$ and ZPE values from Table 1.

Table 3. Experimental Reaction Energies and Enthalpies (kcal mol^{-1}) for Reactions R1a−R2b

property	R1a	R1b	R2a	R2b
$\Delta H_0^{\circ a}$	8.26 ± 0.23	18.15 ± 0.27	−8.87 ± 0.24	1.02 ± 0.28
ΔE^b	9.89 ± 0.63	18.99 ± 0.65	−8.76 ± 0.78	0.34 ± 0.79

[a] ΔH_0° values were derived using the D_0 values from Table 2. [b] ΔE values were derived using the D_e values from Table 2.

set (CBS) limit from augmented quadruple- and quintuple-ζ basis sets (and further refined through the inclusion of relativistic effects and core−valence corrections), using anharmonic ZPE corrections, and combining this data with reliable experimental reference data for all species involved other than CH_3O.[10] The final value reported by Marenich and Boggs for $\Delta_f H_0^\circ(CH_3O)$, 7.36 kcal mol^{-1}, represents the average of the four values obtained for this quantity from each of the four reactions they studied, whereas the uncertainty they attribute to this value, 0.22 kcal mol^{-1}, corresponds to the maximum deviation from this average value.[10] For comparison, the IUPAC critical evaluation[17] for $\Delta_f H_0^\circ(CH_3O)$ is 6.79 ± 0.50 kcal mol^{-1}, which agrees with the value of Marenich and Boggs due to the large uncertainty in this quantity. However, the 0.57 kcal mol^{-1} difference between these two values and the large uncertainties for $\Delta_f H_0^\circ(CH_3O)$ could indicate that there are systematic problems with the calculations and/or with the experiments used to determine this quantity, and choosing one value or the other as our benchmark will affect our results. Because the uncertainty in the value obtained by Marenich and Boggs is smaller, this will provide a stricter benchmark to compare our computations against; therefore, we take the heat of formation and associated uncertainty for the CH_3O radical from the high-level computations of Marenich and Boggs, and we subtract their estimates for the spin-vibronic-zero-point energy (SVZPE = 7905 cm^{-1}) and the Jahn−Teller stabilization energy (JT = 270 cm^{-1}) from the relevant thermochemical quantities to arrive at zero-point-exclusive thermochemistry for the minimum energy structure on the potential energy surface: the $^2A'$ Jahn−Teller minimum.

Finally, because CH_2OH is highly nonrigid and possesses several distinctly anharmonic vibrations, it is difficult to evaluate its ZPE and thermochemistry experimentally. For CH_2OH, we also take these properties (and corresponding uncertainties) from the work of Marenich and Boggs, who incorporated all of the important anharmonic effects into a sophisticated rovibrational Hamiltonian to obtain a measure of the ZPE from the lowest eigenvalue that resulted from the application of this Hamiltonian and to obtain its thermochemistry from the ensuing partition function.[13] We note that, in this case, the IUPAC critical evaluation[17] for $\Delta_f H_0^\circ(CH_2OH)$ is in excellent agreement with the value of Marenich and Boggs.

The thermochemical values and associated 2σ uncertainties used in steps i−iii above are given in Tables 1−3. We note that since Marenich and Boggs did not report any uncertainty for the SVZPE of CH_3O, the 2σ confidence limits we obtained via error propagation for D_e(H−OCH_3) and ΔE for reactions R1b and R2b in Tables 2 and 3 are lower limits to the true 2σ uncertainty.

2.2. Computational Methods. In the first stage of this work, we use electronic model chemistries based on single-level wave function approximations to compute bond energies, reaction energies, and barrier heights for reactions R1a−R2b. Specifically, a variety of coupled cluster approximations are used to compute single-point electronic energies for stationary points optimized (and confirmed by Hessian calculations) with M06-2X/MG3S theory, which has been shown to give reliable geometries.[20,21] A composite approach based on M06-2X/MG3S geometries was also recently used to establish accurate thermochemistry for butoxyl radicals,[22] which are heavier analogues of the methoxyl and hydromethoxyl radicals studied here. The coupled cluster approximations presently used in the first stage are as follows: coupled cluster theory with single and double excitations, CCSD;[23] coupled cluster theory with single and double excitations and a quasiperturbative treatment of connected triple excitations, CCSD(T);[24] coupled cluster theory with single, double, and triple excitations, CCSDT;,[25] and coupled cluster theory with single, double, and triple excitations and a second-order perturbative treatment of quadruple excitations, $CCSDT(2)_Q$.[26]

In the cases of CCSD and CCSD(T), augmented and unaugmented correlation-consistent basis sets—respectively aug-cc-pVnZ and cc-pVnZ (n = D, T, Q)[27−29]—have been used and extrapolated to the complete basis set limit. To obtain the CBS limit, we have used coefficients optimized by Schwenke[30] in two-point extrapolation schemes involving either n = D and T or n = T and Q. The appeal of this extrapolation technique is that it uses a linear superposition ansatz[31] that does not presume that, for any property of interest, the basis set convergence toward the CBS limit should be described by an imposed mathematical functional form, nor does it make the false assumption that the Hartree−Fock reference energy and the coupled cluster correlation energy converge toward their respective CBS limits at the same rate. Instead, these quantities are extrapolated individually

and without presuppositions pertaining to the rate or nature of basis set convergence.

The CBS limits of CCSDT and CCSDT(2)$_Q$ were estimated by adding the energy differences

$$\Delta E(\mathrm{T}) \equiv \mathrm{CCSDT/cc\text{-}pVDZ} - \mathrm{CCSD(T)/cc\text{-}pVDZ}$$

and

$$\Delta E(\mathrm{T2_Q}) \equiv \mathrm{CCSDT(2)_Q/cc\text{-}pVDZ} - \mathrm{CCSD(T)/cc\text{-}pVDZ}$$

to the CCSD(T)/CBS total energies. In addition, wherever indicated, frozen-core and all-electron correlation calculations have been carried out using single-point CCSD(T) calculations with the weighted core−valence triple-ζ basis set cc-pwCVTZ,[32] and the ensuing core−valence corrections (CV) have been applied to all species. Finally, in order to better account for the kinetic energy of electrons near the nuclei, we have computed the mass-velocity and one-electron Darwin scalar relativistic effects (collectively denoted as R) with CISD/cc-pwCVTZ theory on the fixed M06-2X/MG3S geometries using the Cowan−Griffin approach.[33] Therefore, each of the electronic model chemistries can be described by the general model

$$\mathrm{coupled\ cluster/CBS}(n+m) + [\mathrm{CV} + \mathrm{R}]$$

where coupled cluster can be CCSD, CCSD(T), CCSDT, or CCSDT(2)Q; n and m refer to the n- and m-ζ basis sets used in the CBS extrapolation, which we will abbreviate as D, T, and Q for cc-pVDZ, cc-pVTZ, and cc-pVQZ, respectively, and as aD, aT, and aQ for their respective augmented counterparts. The optional quantities in square brackets indicate whether core−valence and scalar relativistic effects have been included.

Because the methods just described are unlikely to be affordable for larger systems of future interest, in the second stage of this analysis, we have investigated whether more efficient approaches, most of which are also based on coupled cluster theory, can also be used to compute the thermochemistry of these reaction systems without significantly compromising the accuracy. Therefore, we eliminate impractical calculations such as those that go beyond the quasiperturbative treatment of triple excitations or the use of basis sets of quadruple-ζ or better quality. Instead, we test the CCSD(T)-F12a[34] and CCSD(T)-F12b[34] explicitly correlated methods, which have been designed to converge with respect to basis sets much more efficiently than calculations with conventional Gaussian basis sets, and in addition to pairing these with T and aT, we will also use them in conjunction with the more efficient jul-cc-pVTZ,[35] which includes diffuse functions on just the non-hydrogenic atoms, and which we will abbreviate as julT in the text, and with maug-cc-pVTZ.[36] We have also used the CBS-QB3[37] multilevel method and the BMC-CCSD[38] and MCG3-MPW[39] multicoefficient correlation methods, the performance-to-cost ratios of which[40] are very appealing given our present scope. As in the previous stage, all calculations in this stage were performed on geometries optimized with M06-2X/MG3S theory.

The density functionals employed in the present article are M05,[41] M05-2X,[42] M06,[20] M06-2X,[20] M08-SO,[43] and M08-HX.[43] The M05-2X, M06-2X, M08-SO, and M08-HX functionals have been shown to provide accurate thermochemistry and barrier heights at a modest computational cost,[21,40,43] whereas the M05 and M06 functionals are interesting because they may provide higher accuracy in cases where multireference character is large. Each of these functionals was paired with several triple-ζ basis sets: MG3S,[44] maug-cc-pVTZ,[36] ma-TZVP,[45−47] and aT. Previous work has shown[35,47] a polarized valence-triple-ζ basis set minimally augmented with diffuse functions—where minimal augmentation is defined as adding diffuse s and p subshells to atoms heavier than hydrogen or helium—is a very suitable basis set for many density functional applications. The MG3S, maug-cc-pVTZ, and ma-TZVP basis sets are examples of minimally augmented basis sets. The ma-TZVP[47] basis set is relatively new; it consists of adding diffuse s and p functions on non-hydrogenic atoms to the def2-TZVP[45,46] basis set.

Coupled cluster calculations were performed with the MOLPRO 2009.1[48] and NWChem[49] program suites. All of the density functional calculations were carried out with a locally modified version of the Gaussian 03 program suite.[50,51] The BMC-CCSD and MCG3-MPW calculations were performed using the MLGAUSS program.[52]

3. RESULTS AND DISCUSSION

3.1. Multireference Diagnostics. Before attempting to treat the present reaction systems with various formalisms based on a single-determinant reference state, it is essential to first assess whether such formalisms are suitable. Many diagnostics have been proposed to provide an approximate measure of mutlti-reference character in the wave function, and in this work, we apply two of them to the methanol reaction systems, namely the T1[53] and GB1[54] diagnostics.

In the case of the T1 diagnostic, the extent of multireference character in a given species is diagnosed by inspecting the amplitudes from single excitations in CCSD calculations, as described by Lee and Taylor.[53] A low T1 value indicates that the wave function is dominated by a single determinant. It has been suggested that the presence of large singles amplitudes is problematic, and, in general, a value in excess of 0.02 for the T1 diagnostic for a closed-shell species indicates that the species in question has significant multireference character.[53] In the case of open-shell species, it has been suggested that a higher threshold for the T1 diagnostic may be more appropriate,[53,55] and several recent studies[56−61] have shown that T1 diagnostic values for open-shell systems of up to ∼0.045 may be acceptable. The T1 diagnostic values for the reactants, products, and transition states of reactions R1a−R2b are given in Table 4. Table 4 reveals that only TS1b has significant multireference character, with a T1 diagnostic value that ranges between 0.47 and 0.57 depending on the basis set used. Thus, the T1 diagnostics suggest that most of the species implicated in reactions R1a−R2b do not possess significant multireference character, indicating that the results obtained for these species via single-reference formalisms should be reliable.

Recently, the GB1 diagnostic has been proposed as a more affordable alternative for assessing the extent of multireference character associated with energetic properties.[54] The GB1 diagnostic is a generalized version of the original B1 diagnostic,[42,62] in which the difference in zero-point-exclusive bond energies obtained with the BLYP[63,64] and B1LYP[65−67] functionals (using geometries optimized with BLYP in both cases) is used as a semiquantitative measure of multireference character—an energetic discrepancy of ∼10 kcal mol^{-1} between the results of these two functionals signifies the presence of considerable multireference character in the D_e in question; in later studies, the same procedure has been advanced as a general criterion for gauging the extent of multireference character "for any quantity with units of energy", which constitutes the GB1 diagnostic.[54]

Table 4. T1 Diagnostics for Species in Reactions R1a−R2b

species	CCSD/cc-pVDZ[a]	CCSD/cc-pVTZ[a]	CCSD/cc-pVQZ[a]	CCSD/aug-cc-pVDZ[a]	CCSD/aug-cc-pVTZ[a]	CCSD/aug-cc-pVQZ[a]
HO_2	0.034	0.034	0.035	0.037	0.036	0.035
HOOH	0.009	0.010	0.010	0.014	0.012	0.012
CH_3OH	0.008	0.008	0.009	0.011	0.010	0.010
CH_2OH	0.018	0.017	0.017	0.019	0.018	0.017
CH_3O	0.017	0.019	0.020	0.021	0.021	0.021
CH_3	0.004	0.005	0.006	0.005	0.006	0.006
CH_4	0.005	0.007	0.008	0.007	0.008	0.008
TS1a	0.018	0.018	0.018	0.020	0.019	0.019
TS1b	0.057	0.049	0.049	0.048	0.047	0.047
TS2a	0.015	0.015	0.015	0.016	0.016	0.015
TS2b	0.021	0.022	0.023	0.023	0.023	0.023

[a] All values were obtained from single-point calculations based on geometries optimized with M06-2X/MG3S.

Table 5. Bond Energies, Reaction Energies, Barrier Heights, B1 Diagnostics, and GB1 Diagnostics in kcal mol^{-1}

property	BLYP/MG3S	B1LYP/MG3S[a]	(G)B1 diagnostic
$D_e(H-OOH)$	87.57	87.65	0.08[b]
$D_e(H-CH_2OH)$	98.76	99.54	0.79[b]
$D_e(H-OCH_3)$	106.01	105.80	0.21[b]
$D_e(H-CH_3)$	109.97	109.55	0.42[b]
ΔE(R1a)	11.19	11.90	0.71[c]
ΔE(R1b)	18.45	18.15	0.29[c]
ΔE(R2a)	−11.21	−10.00	1.21[c]
ΔE(R2b)	−3.95	−3.75	0.21[c]
$V_f^{\ddagger}$(R1a)	9.80	15.66	5.86[c]
$V_f^{\ddagger}$(R1b)[d]	9.88	17.62	7.74[c]
$V_f^{\ddagger}$(R2a)	8.15	12.30	4.14[c]
$V_f^{\ddagger}$(R2b)	5.18	10.22	5.04[c]
$V_r^{\ddagger}$(R1a)	−1.39	3.77	5.15[c]
$V_r^{\ddagger}$(R1b)[d]	−8.64	−0.44	8.21[c]
$V_r^{\ddagger}$(R2a)	19.36	22.30	2.93[c]
$V_r^{\ddagger}$(R2b)	9.13	13.96	4.83[c]

[a] B1LYP/MG3S//BLYP/MG3S. [b] B1. [c] GB1. [d] TS1b could not be located with BLYP/MG3S, so the B1 diagnostic has been performed on B1LYP/MG3S geometries for these barrier heights (see section 3.1).

The rationale behind this diagnostic comes from observations made in previous studies,[42,62] which concluded that "the Hartree−Fock [HF] exchange approximation fails badly for multireference systems, whereas GGAs can usually handle these systems almost as well as they handle single-reference systems." In the case of the GB1 diagnostic, the difference between the performances of the BLYP local functional (i.e., no HF exchange) and the B1LYP hybrid functional (25% of HF exchange) serves as the indicator of multireference character.

Table 5 summarizes the results of the B1 diagnostic for the four bond energies in question and the results of the GB1 diagnostic for the four reaction energies, four forward barrier heights, and four reverse barrier heights considered in this study. We have followed the convention used in the past to calculate these diagnostics, i.e., taking the absolute difference between energetic processes of interest computed with BLYP/MG3S and B1LYP/MG3S//BLYP/MG3S as the value of the diagnostic, except in the cases of $V_f^{\ddagger}$(R1b) and $V_r^{\ddagger}$(R1b), where, because TS1b could not be located with BLYP/MG3S, we used B1LYP/MG3S geometries instead. The results of the B1 and GB1 diagnostics in Table 5 suggest that all of the bonds being broken or formed in the four methanol reactions and the reaction energies for reactions R1a−R2b are suitable for investigations with single-reference methods: the B1/GB1 diagnostics for all of these processes are considerably less than 10 kcal mol^{-1}. The GB1 values for forward and reverse barrier heights are appreciably larger than those for bond and reaction energies; however, all of these are at least 1.79 kcal mol^{-1} below the approximate 10 kcal mol^{-1} threshold for significant multireference character, which indicates that single-reference formalisms can be used in these cases as well.

Therefore, the results of the two approximate multireference diagnostic analyses, the T1 and (G)B1 diagnostics, suggest that single-reference methods can be applied to reliably characterize the present reaction systems.

3.2. Performance of WFT-Based Electronic Model Chemistries. *3.2.1. Electronic Model Chemistries Extrapolated to CBS Limit.* In this section, we present and discuss the results obtained for bond energies, reaction energies, and barrier heights with coupled cluster methods extrapolated to their respective CBS limits using the two-point extrapolation technique proposed by Schwenke.[30] The results for bond energies are summarized in Table 6. As can be seen from Table 6, all of these electronic model chemistries capture important known trends[68] pertaining to bond strengths in alcohols, such as that the α C−H bond is weaker than the O−H bond in alcohols and that this C−H bond is also weaker than its counterpart in methane due to inductive effects caused by the O-atom. In addition, based on the mean unsigned errors (MUEs) with respect to experiment, it can be seen that several of the coupled cluster approaches achieve high accuracy. We see in Table 6 that even CCSD/CBS electronic model chemistries attain sub-kcal mol^{-1} MUEs. Inclusion of connected triple excitations via the popular quasiperturbative formalism [CCSD(T)] can lead to very accurate computed D_e values when extrapolating from T and Q basis sets, but not if D and T basis sets are employed in extrapolating to the CBS limit. In particular, we note that, among the CCSD(T) approaches, CCSD(T)/CBS(T+Q) achieves excellent agreement with experiment for all four D_e values and has an MUE of just 0.10 kcal mol^{-1}. Using aT and aQ basis sets with CCSD(T) slightly increased the MUE to 0.22 kcal mol^{-1}, and the inclusion of CV and R effects did not appreciably affect the CCSD(T) results.

Table 6. Performance of Electronic Model Chemistries Based on Coupled Cluster Theory Extrapolated to CBS Limit for Bond Energies

	bond energy (D_e) (kcal mol^{-1})				
electronic model chemistry[a]	H−OOH	H−CH_2OH	H−OCH_3	H−CH_3	MUE[b]
CCSD/CBS(D+T)	94.05	103.89	112.04	112.06	0.40
CCSD/CBS(aD+aT)	93.60	103.73	111.81	112.16	0.47
CCSD/CBS(T+Q)	93.21	103.30	111.78	111.55	0.84
CCSD/CBS(aT+aQ)	93.23	103.08	111.86	111.40	0.90
CCSD(T)/CBS(D+T)	94.79	104.30	113.40	113.06	0.60
CCSD(T)/CBS(aD+aT)	94.40	104.15	113.25	113.18	0.45
CCSD(T)/CBS(T+Q)	93.97	103.72	113.16	112.56	0.10
CCSD(T)/CBS(aT+aQ)	93.98	103.49	113.23	112.40	0.22
CCSD(T)/CBS(T+Q) + CV + R	93.95	103.74	113.14	112.70	0.12
CCSD(T)/CBS(aT+aQ) + CV + R	93.96	103.50	113.21	112.54	0.17
CCSDT/CBS(T+Q)	93.91	103.78	113.14	112.60	0.07
CCSDT/CBS(aT+aQ)	93.92	103.55	113.21	112.44	0.17
CCSDT/CBS(T+Q) + CV + R	93.89	103.80	113.12	112.74	0.10
CCSDT/CBS(aT+aQ) + CV + R	93.90	103.57	113.19	112.58	0.14
CCSDT(2)$_Q$/CBS(T+Q)	93.99	103.80	113.25	112.61	0.12
CCSDT(2)$_Q$/CBS(aT+aQ)	94.00	103.56	113.33	112.45	0.21
CCSDT(2)$_Q$/CBS(T+Q) + CV + R	93.97	103.81	113.24	112.75	0.15
CCSDT(2)$_Q$/CBS(aT+aQ) + CV + R	93.98	103.58	113.31	112.59	0.18
experimental	93.91 ± 0.30	103.80 ± 0.56	112.91 ± 0.57[c]	112.56 ± 0.55	−

[a] All computed values were obtained from single-point calculations based on geometries optimized with M06-2X/MG3S. [b] Mean unsigned errors with respect to the central value of the accepted experimental ranges. [c] The uncertainty attributed to this value is a lower limit of the true 2σ uncertainty (see section 2.1).

Results obtained with CCSDT and CCSDT(2)$_Q$ are very similar for the present reactions to those obtained with CCSD(T): using a CBS(T+Q) extrapolation led to the smallest MUEs (0.07 and 0.12 kcal mol^{-1}, respectively), basis set augmentation seems to be unimportant, and core−valence and scalar relativistic effects only marginally changed the computed D_e values. We note here that while CCSDT slightly outperformed CCSD(T) in terms of MUEs for the present systems, previous work has shown that this need not be the case.[69−75] Experience has shown that when the results of CCSD(T) and CCSDT are appreciably different, neither is reliable for the systems under investigation.[70] However, the fact that the performance of these two theories is so similar in this case suggests that both these coupled cluster approaches are well-suited for characterizing the reaction systems currently explored. Furthermore, the negligible contributions of full triple excitations and second-order perturbative quadruple excitations to the computed D_e values suggest that these quantities are sufficiently converged already at the CCSD(T) level of theory.

The reaction energies computed with CCSD, CCSD(T), CCSDT, and CCSDT(2)$_Q$ are given in Table 7. Highly accurate results are again obtained with the latter three theories, and due to error cancellation, the CCSD ΔE results are also quite reasonable. With the exception of CCSD(T)/CBS(*an*+*am*), the use of T and Q basis sets to extrapolate to the CBS limit led to more accurate results than when using D and T basis sets. The close agreement between CCSD(T), CCSDT, and CCSDT(2)$_Q$ results for ΔE once again shows that the results obtained with CCSD(T) are well converged. The electronic model chemistry with the smallest MUEs are CCSDT/CBS(T+Q) and CCSDT/CBS(T+Q) + CV + R, each with an MUE of 0.12 kcal mol^{-1}, and in all cases, we see that the core−valence and scalar relativistic effects have roughly canceled out and do not considerably impact the results. As was found for D_e, the use of augmented basis sets also seems unnecessary for ΔE, as, in most cases, the use of augmented basis sets to extrapolate to the CBS limit led to slightly larger MUEs.

Finally, in Table 8 we present the coupled cluster results for the forward and reverse barrier heights for reactions R1a−R2b, $V_f^{\ddagger}$ and $V_r^{\ddagger}$, respectively. The MUEs in Table 8 are in reference to our best level of theory: CCSDT(2)$_Q$/CBS(aT+aQ) + CV + R. Table 8 shows that the use of CCSD theory leads to substantial overestimations of the forward and reverse barrier heights for all four reactions considered. The lowest level of theory that can be used to yield reasonable agreement with our best estimates for barrier heights is CCSD(T) theory extrapolated to the CBS limit from T and Q basis sets. The use of augmented basis sets as opposed to unaugmented basis sets to extrapolate to the CBS limit does, in some cases, lead to nonnegligible differences in barrier heights; for example, for CCSDT(2)$_Q$ theory this difference is 0.22 kcal mol^{-1} for $V_f^{\ddagger}$(R2b), 0.35 kcal mol^{-1} for $V_r^{\ddagger}$(R1a), and 0.25 kcal mol^{-1} for $V_r^{\ddagger}$(R2a). However, it appears that once again core−valence and scalar relativistic effects can be safely neglected.

3.2.2. Tests of More Efficient Electronic Model Chemistries. The use of coupled cluster theory with full connected triple excitations or beyond, or even the use of CCSD(T) theory with an augmented quadruple-ζ basis set, is highly impractical for complex systems and likely computationally unaffordable for the butanol combustion reactions we plan to study in the near future. We have already found in section 3.2.1 that while CCSD theory is inadequate for accurately characterizing the reaction systems

Table 7. Performance of Electronic Model Chemistries Based on Coupled Cluster Theory Extrapolated to CBS Limit for Reaction Energies

	reaction energy (ΔE) (kcal mol^{-1})				
electronic model chemistry[a]	R1a	R1b	R2a	R2b	MUE[b]
CCSD/CBS(D+T)	9.84	17.99	−8.18	−0.03	0.50
CCSD/CBS(aD+aT)	10.13	18.21	−8.43	−0.35	0.51
CCSD/CBS(T+Q)	10.09	18.57	−8.25	0.23	0.31
CCSD/CBS(aT+aQ)	9.84	18.63	−8.32	0.47	0.24
CCSD(T)/CBS(D+T)	9.51	18.61	−8.76	0.34	0.19
CCSD(T)/CBS(aD+aT)	9.75	18.85	−9.03	0.07	0.20
CCSD(T)/CBS(T+Q)	9.75	19.19	−8.83	0.60	0.17
CCSD(T)/CBS(aT+aQ)	9.51	19.25	−8.91	0.83	0.32
CCSD(T)/CBS(T+Q) + CV + R	9.79	19.19	−8.96	0.44	0.15
CCSD(T)/CBS(aT+aQ) + CV + R	9.54	19.25	−9.04	0.67	0.30
CCSDT/CBS(T+Q)	9.87	19.23	−8.82	0.54	0.12
CCSDT/CBS(aT+aQ)	9.63	19.29	−8.89	0.77	0.28
CCSDT/CBS(T+Q) + CV + R	9.90	19.23	−8.95	0.38	0.12
CCSDT/CBS(aT+aQ) + CV + R	9.66	19.29	−9.02	0.61	0.26
CCSDT(2)$_Q$/CBS(T+Q)	9.81	19.27	−8.81	0.65	0.18
CCSDT(2)$_Q$/CBS(aT+aQ)	9.57	19.33	−8.88	0.88	0.33
CCSDT(2)$_Q$/CBS(T+Q) + CV + R	9.84	19.27	−8.94	0.49	0.16
CCSDT(2)$_Q$/CBS(aT+aQ) + CV + R	9.60	19.33	−9.01	0.72	0.31
experimental	9.89 ± 0.63	18.99 ± 0.65[c]	−8.76 ± 0.78	0.34 ± 0.79[c]	–

[a] All computed values were obtained from single-point calculations based on geometries optimized with M06-2X/MG3S. [b] Mean unsigned errors with respect to the central value of the accepted experimental ranges. [c] The uncertainty attributed to this value is a lower limit of the true 2σ uncertainty (see section 2.1).

Table 8. Performance of Electronic Model Chemistries Based on Coupled Cluster Theory Extrapolated to CBS Limit for Barrier Heights

	forward barrier height ($V_f^{\ddagger}$) (kcal mol^{-1})				reverse barrier height ($V_r^{\ddagger}$) (kcal mol^{-1})				
electronic model chemistry[a]	R1a	R1b	R2a	R2b	R1a	R1b	R2a	R2b	MUE[b]
CCSD/CBS(D+T)	20.37	25.72	16.22	16.24	10.53	7.74	24.40	16.26	2.74
CCSD/CBS(aD+aT)	20.54	25.77	15.92	16.02	10.41	7.56	24.35	16.37	2.67
CCSD/CBS(T+Q)	20.88	26.77	16.07	16.65	10.79	8.21	24.32	16.42	3.07
CCSD/CBS(aT+aQ)	20.96	26.91	16.23	16.86	11.12	8.28	24.55	16.40	3.22
CCSD(T)/CBS(D+T)	16.30	22.43	13.68	13.35	6.79	3.82	22.44	13.01	0.47
CCSD(T)/CBS(aD+aT)	16.42	22.49	13.35	13.13	6.66	3.63	22.38	13.06	0.56
CCSD(T)/CBS(T+Q)	16.76	23.44	13.52	13.74	7.01	4.25	22.35	13.13	0.17
CCSD(T)/CBS(aT+aQ)	16.87	23.61	13.69	13.96	7.36	4.36	22.60	13.12	0.05
CCSD(T)/CBS(T+Q) + CV + R	16.89	23.51	13.56	13.70	7.10	4.32	22.52	13.25	0.12
CCSD(T)/CBS(aT+aQ) + CV + R	17.00	23.69	13.73	13.92	7.46	4.43	22.77	13.24	0.08
CCSDT/CBS(T+Q)	16.97	23.38	13.55	13.79	7.10	4.15	22.37	13.25	0.17
CCSDT/CBS(aT+aQ)	17.08	23.55	13.73	14.01	7.46	4.26	22.62	13.24	0.10
CCSDT/CBS(T+Q) + CV + R	17.10	23.45	13.59	13.75	7.19	4.23	22.53	13.37	0.15
CCSDT/CBS(aT+aQ) + CV + R	17.21	23.63	13.76	13.97	7.55	4.34	22.78	13.36	0.13
CCSDT(2)$_Q$/CBS(T+Q)	16.68	23.40	13.47	13.67	6.87	4.14	22.28	13.03	0.25
CCSDT(2)$_Q$/CBS(aT+aQ)	16.79	23.57	13.65	13.89	7.23	4.25	22.53	13.02	0.09
CCSDT(2)$_Q$/CBS(T+Q) + CV + R	16.81	23.48	13.51	13.63	6.97	4.21	22.45	13.15	0.18
CCSDT(2)$_Q$/CBS(aT+aQ) + CV + R	16.92	23.65	13.69	13.85	7.32	4.32	22.70	13.14	–

[a] All computed values were obtained from single-point calculations based on geometries optimized with M06-2X/MG3S. [b] Mean unsigned errors are with respect to the best level of theory: CCSDT(2)$_Q$/CBS(aT+aQ) + CV + R//M06-2X/MG3S.

presently studied, it is not necessary to go beyond CCSD(T)/CBS(T+Q) to obtain well-converged accurate thermochemistry and barrier heights for the reactions in this paper. We now explore if a similar degree of accuracy can be achieved without

Table 9. Performance of Efficient WFT-Based Electronic Model Chemistries for Bond Energies

	bond energy (D_e) (kcal mol^{-1})				
electronic model chemistry[a]	H−OOH	H−CH_2OH	H−OCH_3	H−CH_3	MUE[b]
CCSD(T)/cc-pVTZ	91.67	102.23	110.52	111.28	1.87
CCSD(T)/maug-cc-pVTZ	92.29	102.37	111.10	111.04	1.59
CCSD(T)/jul-cc-pVTZ	92.37	102.52	111.13	111.23	1.48
CCSD(T)/aug-cc-pVTZ	92.71	102.71	111.34	111.36	1.27
CCSD(T)-F12a/cc-pVTZ	93.35	103.54	112.82	112.76	0.28
CCSD(T)-F12a/maug-cc-pVTZ	93.96	103.58	113.18	112.50	0.15
CCSD(T)-F12a/jul-cc-pVTZ	93.79	103.58	113.02	112.50	0.13
CCSD(T)-F12a/aug-cc-pVTZ	93.93	103.59	113.09	112.48	0.12
CCSD(T)-F12b/cc-pVTZ	92.97	103.28	112.45	112.51	0.49
CCSD(T)-F12b/maug-cc-pVTZ	93.57	103.31	112.81	112.25	0.31
CCSD(T)-F12b/jul-cc-pVTZ	93.44	103.31	112.69	112.25	0.37
CCSD(T)-F12b/aug-cc-pVTZ	93.60	103.34	112.77	112.24	0.31
CCSD(T)-F12a/jul-cc-pVTZ + CV + R	93.77	103.59	113.00	112.64	0.13
CCSD(T)-F12a/aug-cc-pVTZ + CV + R	93.91	103.60	113.07	112.62	0.10
CCSD(T)-F12b/jul-cc-pVTZ + CV + R	93.42	103.32	112.67	112.39	0.34
CCSD(T)-F12b/aug-cc-pVTZ + CV + R	93.58	103.35	112.75	112.38	0.28
BMC-CCSD	94.35	103.91	115.06	113.09	0.81
MCG3-MPW	93.36	103.11	112.89	112.34	0.37
CBS-QB3	94.11	104.02	113.19	113.11	0.31

[a] All computed values were obtained from single-point calculations based on geometries optimized with M06-2X/MG3S. [b] Mean unsigned errors with respect to the central value of the accepted experimental ranges.

having to employ a costly quadruple-ζ basis set. Therefore, the first test for a more efficient electronic model chemistry is to assess the feasibility of just using CCSD(T) with a triple-ζ basis set—T, maug-cc-pVTZ, julT, or aT—to compute accurate thermochemistry and barrier heights. For very little additional computational cost, it is also possible to use the CCSD(T)-F12a and CCSD(T)-F12b explicitly correlated formalisms, which were designed to recover a substantially larger fraction of the correlation energy than standard CCSD(T) with the same basis set.[34] As such, these explicitly correlated coupled cluster approaches should be quite accurate when paired with even just a triple-ζ basis set. Finally, we also explore the accuracy of the highly cost-efficient BMC-CCSD, MCG3-MPW, and CBS-QB3 multilevel methods, modified to use M06-2X/MG3S geometries for consistency. The results obtained with these electronic model chemistries for bond energies, reaction energies, and barrier heights are given in Tables 9, 10, and 11, respectively.

We see from Table 9 that standard CCSD(T) paired with any of the triple-ζ basis sets considered is inadequate for accurately describing the bond energies for the four bonds of interest, yielding MUEs in excess of 1 kcal mol^{-1} in each case. In the present case, BMC-CCSD has an unusually large MUE of 0.81 kcal mol^{-1}, which can be largely attributed to its considerable overestimation of the O−H bond strength in methanol. CCSD(T)-F12b/T achieves an MUE below half a kilocalorie per mole, 0.49 kcal mol^{-1}, and this value is further reduced to 0.31 kcal mol^{-1} by minimally augmenting with diffuse functions (that is, adding diffuse s and p functions on all non-hydrogen atoms) via the maug-cc-pVTZ basis set. No further improvement is gained by using julT or the much more inefficient aT basis set in conjunction with CCSD(T)-F12b, which yield respective MUEs of 0.37 and 0.31 kcal mol^{-1}, indicating that going beyond the minimally augmented basis set prescription is unnecessary for the present cases. We also note that a similar degree of accuracy is achieved by the much more affordable MCG3-MPW and CBS-QB3 methods, yielding respective MUEs of just 0.37 and 0.31 kcal mol^{-1}.

Finally, we remark that the results obtained with CCSD(T)-F12a are quite good for the bond energies considered. Using no augmentation on the triple-ζ basis set accompanying CCSD(T)-F12a leads to an MUE of 0.28 kcal mol^{-1}; however, minimally augmenting with diffuse functions on heavy atoms reduces this value to a remarkable 0.15 kcal mol^{-1} for maug-cc-pVTZ. Little further improvement is gained from including additional s and p diffuse functions via julT or by also including diffuse functions on hydrogen atoms via aT, MUEs = 0.13 and 0.12 kcal mol^{-1}, respectively. Because CV and R single-point calculations are not very costly, we have also included these effects for all CCSD(T)-F12 calculations with julT and aT, and we find that this procedure leads to only marginal or no improvement (Table 9).

We now turn our attention to the results for reaction energies in Table 10. We see that the systematic underestimation of the bond energies by standard CCSD(T) theory leads to fortuitous error cancellation in the case of reaction energies, leading to MUEs of 0.55, 0.19, 0.25, and 0.24 kcal mol^{-1}, with T, maug-cc-pVTZ, julT, and aT, respectively. This is not the case for BMC-CCSD, where because of the poor characterization of D_e(H−OCH_3) the ensuing reaction energies also have an unusually large MUE value: 1.03 kcal mol^{-1}. MCG3-MPW also performs quite well on this front, having an MUE of 0.34 kcal mol^{-1}, which is slightly better than the MUEs achieved by either CCSD(T)-F12a or CCSD(T)-F12b in conjunction with the T basis set: 0.38 and 0.44 kcal mol^{-1}, respectively. The reaction energies obtained with CBS-QB3 for the present reactions are quite good: MUE = 0.18 kcal mol^{-1}. Both CCSD(T)-F12a and CCSD(T)-F12b perform quite well when accompanied by basis sets which

Table 10. Performance of Efficient WFT-Based Electronic Model Chemistries for Reaction Energies

	reaction energy (ΔE) (kcal mol^{-1})				
electronic model chemistry[a]	R1a	R1b	R2a	R2b	MUE[b]
CCSD(T)/cc-pVTZ	10.56	18.85	−9.04	−0.76	0.55
CCSD(T)/maug-cc-pVTZ	10.08	18.81	−8.68	0.06	0.19
CCSD(T)/jul-cc-pVTZ	10.15	18.76	−8.71	−0.10	0.25
CCSD(T)/aug-cc-pVTZ	10.00	18.63	−8.65	−0.02	0.24
CCSD(T)-F12a/cc-pVTZ	10.19	19.47	−9.22	0.06	0.38
CCSD(T)-F12a/maug-cc-pVTZ	9.63	19.22	−8.92	0.67	0.24
CCSD(T)-F12a/jul-cc-pVTZ	9.79	19.23	−8.92	0.52	0.17
CCSD(T)-F12a/aug-cc-pVTZ	9.66	19.16	−8.89	0.61	0.20
CCSD(T)-F12b/cc-pVTZ	10.30	19.48	−9.23	−0.06	0.44
CCSD(T)-F12b/maug-cc-pVTZ	9.74	19.24	−8.94	0.56	0.19
CCSD(T)-F12b/jul-cc-pVTZ	9.87	19.25	−8.94	0.44	0.14
CCSD(T)-F12b/aug-cc-pVTZ	9.74	19.17	−8.90	0.53	0.16
CCSD(T)-F12a/jul-cc-pVTZ + CV + R	9.82	19.23	−9.05	0.36	0.15
CCSD(T)-F12a/aug-cc-pVTZ + CV + R	9.69	19.16	−9.02	0.45	0.18
CCSD(T)-F12b/jul-cc-pVTZ + CV + R	9.90	19.25	−9.07	0.28	0.16
CCSD(T)-F12b/aug-cc-pVTZ + CV + R	9.77	19.18	−9.03	0.37	0.15
BMC-CCSD	9.56	20.72	−9.18	1.97	1.03
MCG3-MPW	9.75	19.53	−9.23	0.55	0.34
CBS-QB3	9.91	19.08	−9.10	0.07	0.18

[a] All computed values were obtained from single-point calculations based on geometries optimized with M06-2X/MG3S. [b] Mean unsigned errors with respect to the central value of the accepted experimental ranges.

Table 11. Performance of Efficient WFT-Based Electronic Model Chemistries for Barrier Heights

	forward barrier height ($V_f^{\ddagger}$) (kcal mol^{-1})				reverse barrier height ($V_r^{\ddagger}$) (kcal mol^{-1})				
electronic model chemistry[a]	R1a	R1b	R2a	R2b	R1a	R1b	R2a	R2b	MUE[b]
CCSD(T)/cc-pVTZ	16.92	22.73	13.69	13.01	6.36	3.88	22.73	13.76	0.48
CCSD(T)/maug-cc-pVTZ	17.41	23.55	13.96	13.65	7.34	4.73	22.64	13.59	0.25
CCSD(T)/jul-cc-pVTZ	16.77	23.03	13.59	13.22	6.63	4.28	22.30	13.32	0.35
CCSD(T)/aug-cc-pVTZ	16.36	22.55	13.33	13.01	6.36	3.92	21.97	13.03	0.63
CCSD(T)-F12a/cc-pVTZ	16.10	22.44	13.16	13.25	5.91	2.98	22.38	13.20	0.78
CCSD(T)-F12a/maug-cc-pVTZ	16.73	23.27	13.52	13.85	7.10	4.05	22.44	13.18	0.19
CCSD(T)-F12a/jul-cc-pVTZ	16.76	23.30	13.49	13.73	6.98	4.06	22.41	13.21	0.22
CCSD(T)-F12a/aug-cc-pVTZ	16.66	23.17	13.46	13.74	7.01	4.02	22.35	13.13	0.26
CCSD(T)-F12b/cc-pVTZ	16.28	22.60	13.23	13.20	5.98	3.12	22.46	13.25	0.71
CCSD(T)-F12b/maug-cc-pVTZ	16.91	23.42	13.59	13.79	7.17	4.18	22.53	13.24	0.12
CCSD(T)-F12b/jul-cc-pVTZ	16.89	23.41	13.53	13.68	7.02	4.16	22.47	13.25	0.17
CCSD(T)-F12b/aug-cc-pVTZ	16.78	23.27	13.48	13.67	7.04	4.10	22.38	13.14	0.22
CCSD(T)-F12a/jul-cc-pVTZ + CV + R	16.89	23.37	13.52	13.69	7.07	4.14	22.57	13.33	0.17
CCSD(T)-F12a/aug-cc-pVTZ + CV + R	16.79	23.25	13.50	13.70	7.10	4.09	22.52	13.25	0.20
CCSD(T)-F12b/jul-cc-pVTZ + CV + R	17.02	23.49	13.56	13.64	7.11	4.24	22.64	13.37	0.15
CCSD(T)-F12b/aug-cc-pVTZ + CV + R	16.90	23.35	13.52	13.63	7.13	4.17	22.55	13.26	0.16
BMC-CCSD	17.30	24.29	13.40	14.26	7.74	3.58	22.58	12.29	0.48
MCG3-MPW	16.57	23.20	13.04	13.29	6.82	3.67	22.27	12.74	0.50
CBS-QB3	15.34	22.44	12.96	12.43	5.43	3.36	22.06	12.36	1.15

[a] All computed values were obtained from single-point calculations based on geometries optimized with M06-2X/MG3S. [b] Mean unsigned errors are with respect to the best level of theory: CCSDT(2)$_Q$/CBS(aT+aQ) + CV + R//M06-2X/MG3S.

include diffuse functions. In the case of maug-cc-pVTZ, the respective MUEs for CCSD(T)-F12a and CCSD(T)-F12b are 0.24 and 0.19 kcal mol^{-1}, for julT, the ensuing MUEs are 0.17 and 0.14 kcal mol^{-1} for CCSD(T)-F12a and CCSD(T)-F12b, respectively, and when using aT, these respective MUE values slightly increase to 0.20 and 0.16 kcal mol^{-1}. These findings further suggest that while it is important to include diffuse functions on heavy atoms, the inclusion of diffuse functions on

dx.doi.org/10.1021/jp110024e |J. Phys. Chem. A 2011, 115, 2811–2829

Table 12. Performance of Minnesota Density Functionals for Barrier Heights and Reaction Energies

	forward barrier height ($V_f^{\ddagger}$) (kcal mol^{-1})				reverse barrier height ($V_r^{\ddagger}$) (kcal mol^{-1})				reaction energy (ΔE) (kcal mol^{-1})				
electronic model chemistry[a]	R1a	R1b	R2a	R2b	R1a	R1b	R2a	R2b	R1a	R1b	R2a	R2b	MUE[b]
M05/MG3S	15.89	19.19	12.94	12.28	3.84	−0.61	22.75	14.34	12.05	19.80	−9.80	−2.06	1.99
M05-2X/MG3S	15.26	21.60	12.69	11.74	4.11	1.90	22.30	12.79	11.15	19.70	−9.61	−1.05	1.45
M06/MG3S	13.75	16.57	11.99	11.53	3.33	−1.50	21.44	13.32	10.42	18.08	−9.45	−1.79	2.48
M06-2X/MG3S	14.65	20.07	12.41	11.61	4.11	1.17	21.80	12.64	10.54	18.90	−9.39	−1.03	1.66
M08-SO/MG3S	16.66	21.74	13.48	13.13	6.06	1.93	22.80	13.24	10.60	19.81	−9.32	−0.11	0.79
M08-HX/MG3S	15.69	22.08	13.00	13.36	5.94	2.95	22.89	13.87	9.75	19.13	−9.89	−0.51	0.83
M05-2X/ma-TZVP	15.73	21.97	12.72	11.44	3.97	1.95	22.37	12.84	11.77	20.02	−9.65	−1.40	1.51
M06-2X/ma-TZVP	15.25	20.65	12.59	11.51	4.20	1.53	21.97	12.82	11.06	19.12	−9.38	−1.31	1.55
M08-SO/ma-TZVP	17.96	22.48	13.62	12.78	6.16	2.39	23.08	13.96	11.80	20.09	−9.46	−1.18	1.07
M08-HX/ma-TZVP	16.84	23.00	13.13	13.20	6.26	3.52	23.13	14.30	10.58	19.48	−10.00	−1.10	0.77
M05-2X/maug-cc-pVTZ	15.24	21.57	12.96	11.88	4.51	2.03	22.36	12.47	10.72	19.53	−9.40	−0.59	1.29
M06-2X/maug-cc-pVTZ	14.74	20.22	12.67	11.82	4.59	1.45	21.92	12.45	10.15	18.77	−9.25	−0.63	1.47
M08-SO/maug-cc-pVTZ	17.55	22.46	13.63	13.17	6.58	2.46	23.06	13.56	10.97	20.00	−9.43	−0.39	0.79
M08-HX/maug-cc-pVTZ	16.12	22.43	13.36	13.57	6.56	3.38	23.08	13.80	9.56	19.05	−9.72	−0.23	0.61
M05-2X/aug-cc-pVTZ	15.13	21.45	12.95	11.88	4.47	1.97	22.30	12.40	10.65	19.48	−9.34	−0.52	1.31
M06-2X/aug-cc-pVTZ	14.67	20.15	12.63	11.79	4.56	1.40	21.86	12.39	10.11	18.74	−9.23	−0.60	1.50
M08-SO/aug-cc-pVTZ	17.43	22.32	13.53	13.06	6.51	2.34	23.02	13.49	10.92	19.98	−9.49	−0.43	0.81
M08-HX/aug-cc-pVTZ	16.00	22.27	13.24	13.48	6.51	3.24	23.04	13.74	9.49	19.03	−9.80	−0.26	0.67

[a] Geometries for all DFT calculations in this article are obtained consistently; e.g., M08-HX/aug-cc-pVTZ calculations employ M08-HX/aug-cc-pVTZ geometries. [b] Mean unsigned errors are with respect to best estimates: experiment for ΔE and CCSDT(2)$_Q$/CBS(aT+aQ) + CV + R//M06-2X/MG3S for $V_f^{\ddagger}$ and $V_r^{\ddagger}$.

hydrogen atoms is superfluous for the reaction energies of reactions R1a−R2b. Finally, as was also found for bond energies, we found that CV and R corrections affect the reaction energies of the present systems only slightly.

Our final test for this subgroup of electronic model chemistries is reaction barrier heights. The computed forward and reverse barrier heights and overall MUE for both sets of barrier heights are presented in Table 11. Although Table 11 does not consider reaction energies explicitly, in what follows it should be clear that one cannot obtain accurate values for both the forward and reverse barriers if the reaction energies are not accurate; therefore, reaction energies are included implicitly. The performance of electronic model chemistries with regard to reaction barrier heights is of critical importance because rate coefficients computed with transition state theory depend on barrier heights exponentially. The MUE values in Table 11 are in reference to the barrier heights computed with our best level of theory: CCSDT(2)$_Q$/CBS(aT+aQ) + CV + R//M06-2X/MG3S. Remarkably, all the electronic model chemistries tested, with the exception of CBS-QB3, achieve MUEs of less than 1 kcal mol^{-1}. Once again, the CCSD(T)-F12 methods significantly outperform CCSD(T) if augmented triple-ζ basis sets are used; however, we note that this is not the case if just the T basis set is used. Both multicoefficient electronic model chemistries tested perform very satisfactorily, with MUEs of 0.48 and 0.50 kcal mol^{-1} for BMC-CCSD and MCG3-MPW, respectively. Both CCSD(T)-F12a and CCSD(T)-F12b attain very accurate barrier heights when paired with either the maug-cc-pVTZ, julT, or aT basis sets, with MUEs in the range of 0.19−0.26 kcal mol^{-1} for the former method and 0.12−0.22 kcal mol^{-1} for the latter, with a slight edge going to maug-cc-pVTZ in both cases. Including CV and R effects reduces the MUE by no more than 0.06 kcal mol^{-1} in all cases.

3.3. Performance of DFT-Based Electronic Model Chemistries. *3.3.1. Reaction Energies and Barrier Heights.* We now assess the performance of the six density functionals with regard to barrier heights and reaction energies, but we no longer consider bond energies since these are not directly relevant for our future dynamics calculations. Thus, our goal is to find a combination of density functional and one-electron basis set that can achieve an overall MUE of less than 1 kcal mol^{-1} and use it in future work for a direct dynamics study of the above methanol reactions using variational transition state theory and multidimensional tunneling.

Preliminary calculations indicated that while the geometries and energetics computed with the density functionals considered in this work do not change appreciably with the size of the integration grid used to compute them, the computed vibrational frequencies are sensitive to the size of the integration grid. To further explore this issue, we recomputed the geometries, energetics, and vibrational frequencies obtained with the largest and most expensive integration grid available in Gaussian, (96,32,64), which denotes the placement of 960 radial shells around each atom and a spherical product grid composed of 32 radial points and 64 angular points per shell; the keyword for requesting this massive grid is Int(Grid=-96032). The results of this integration-grid-convergence analysis showed that, for all DFT-based electronic model chemistries considered in this work, numerical convergence is reached for all properties considered if employing an integration grid consisting of 99 radial shells around each atom and 770 angular points in each shell (99,770). Therefore, all of the results presented in this work have been obtained using this integration grid.

In the past, the Minnesota functionals have frequently been employed with the efficient MG3S basis set, which is a minimally augmented valence-triple-ζ basis set, and we begin here by using this basis set as well. Table 12 considers both barrier heights and reaction energies. We see from the results in Table 12, that when paired with MG3S, M05 and M06 have the largest MUEs (≥1.99

Table 13. Improved DFT Results for Reaction Energies and Barrier Heights of Reactions R1a and R1b via Specific-Reaction Parametrization

	forward barrier height ($V_f^{\ddagger}$) (kcal mol^{-1})		reverse barrier height ($V_r^{\ddagger}$) (kcal mol^{-1})		reaction energy (ΔE) (kcal mol^{-1})		
electronic model chemistry	R1a	R1b	R1a	R1b	R1a	R1b	MUE[a]
M08-HX/maug-cc-pVTZ	16.12	22.43	6.56	3.38	9.56	19.05	0.68
M08-HX54/maug-cc-pVTZ	16.66	23.23	7.27	4.10	9.40	19.13	0.26
M08-HX55/maug-cc-pVTZ	16.97	23.68	7.67	4.51	9.30	19.17	0.23
M08-HX56/maug-cc-pVTZ	17.27	24.13	8.08	4.92	9.20	19.21	0.52
M08-HX57/maug-cc-pVTZ	17.58	24.59	8.48	5.34	9.09	19.25	0.80

[a] Mean unsigned errors are with respect to best estimates: experiment for ΔE and CCSDT(2)$_Q$/CBS(aT+aQ) + CV + R//M06-2X/MG3S for $V_f^{\ddagger}$ and $V_r^{\ddagger}$.

kcal mol^{-1}), that the MUEs of M05-2X and M06-2X are well below 2 kcal mol^{-1}, and that using the latest generation of Minnesota density functionals, M08-SO and M08-HX, leads to sub-kcal mol^{-1} MUEs. The fact that M05 and M06 are outperformed by their 2X counterparts, which contain twice the percentages of Hartree−Fock exchange, further indicates that the reactions studied here are not significantly affected by multireference effects, because in the cases characterized by significant multireference character, one would expect increasing the fraction of HF exchange to diminish the quality of the results.[54,62,76] Based on these findings, the M05 and M06 functionals are not considered further.

The overall level of accuracy achieved by the Minnesota functionals with the MG3S basis set for barrier heights surpasses that attained by CCSD extrapolated to the CBS limit. Moreover, the M08 class of density functionals performs about as well with the MG3S basis set as CCSD(T) with the T or aT basis sets for barrier heights, at a small fraction of the computational cost. Still, it is important to test if the performance of these M08 functionals, M05-2X, and M06-2X, can be further improved by changing the nature of the triple-ζ basis set. Table 12 shows the effects of changing the basis set on the barrier heights and reaction energies computed with the various density functional approximations. The results can be summarized as follows: using the ma-TZVP basis set slightly increased the MUEs for M05-2X and M08-SO while slightly decreasing the MUEs for M06-2X and M08-HX; using maug-cc-pVTZ led to the lowest MUEs for all functionals; using aT led to MUEs that were generally better than those obtained with MG3S or ma-TZVP, but slightly larger than those obtained with maug-cc-pVTZ in each case. *Overall, the best performance was for M08-HX/maug-cc-pVTZ, which achieves an MUE of just 0.61 kcal mol^{-1} for reaction energies and barrier heights.*

3.3.2. Improved DFT Performance via Specific-Reaction Parametrization. A closer inspection of Table 12 reveals that while the forward and reverse barrier heights for reactions R2a and R2b are accurately computed with the electronic model chemistry found to give the best performance for the reactions considered in this work, M08-HX/maug-cc-pVTZ (with deviations in the range 0.3−0.7 kcal mol^{-1}), the forward and reverse barrier heights for reactions R1a and R1b are systematically underestimated by 0.8−1.2 kcal mol^{-1} with this electronic model chemistry. These systematic underestimations fortuitously largely cancel in the calculation of reaction energies. Previous work[77] has shown that the systematic underestimation of barrier heights for a specific reaction by DFT can be corrected by increasing the amount of HF exchange in the hybrid functional—which is consistent in a sense with HF theory generally overpredicting barrier heights,[40,78,79] although it is not quite that straightforward because HF theory has no correlation functional. Based on the sensitivity of calculated barrier heights to the percentage of Hartree−Fock exchange, our aim is to improve the performance of M08-HX/maug-cc-pVTZ for reactions R1a and R1b via specific-reaction parametrization, i.e., empirically increasing the percentage (X) of HF exchange while keeping all other parameters the same in M08-HX.

The percentage of HF exchange in standard M08-HX is 52.29%, which for reactions R1a and R1b leads to an MUE of 0.68 kcal mol^{-1} for reaction energies and barrier heights (Table 13). Systematic modification of X showed that the MUE is reduced to 0.23 kcal mol^{-1} for the reaction energies and barrier heights of reactions R1a and R1b if the amount of HF exchange in M08-HX is slightly raised to 55% (Table 13). We have carried out this procedure in Gaussian 03[50] by simply adding the IOp(3/76=*nnnnnmmmmm*) keyword to the route section of an otherwise typical M08-HX input file, where *nnnnn* is set to 10000 and *mmmmm* corresponds to the fractional value of X multiplied by 10000 and preceded by a 0, e.g., 05500 in the case of 55% HF exchange and 05229 for standard M08-HX. We denote this modified electronic model chemistry based on 55% HF exchange as M08-HX55/maug-cc-pVTZ, and plan to use it in the future direct dynamics studies of reactions R1a and R1b; standard M08-HX/maug-cc-pVTZ will be used for the dynamics calculations of reactions R2a and R2b.

3.3.3. Geometries. The geometries of the reactants and products of reactions R1a−R2b optimized with the various DFT-based electronic model chemistries used in this study are given in the Supporting Information and depicted in Figure 1. A comparison of the computed structural parameters of the reactants and products of reactions R1a−R2b and their experimental counterparts is presented in Table 14. For brevity, the comparison in Table 14 was confined to just a representative subset of the DFT-based electronic model chemistries employed in this work, and we have not included any of the geometries obtained with the aT basis set since the results obtained with this basis set are so similar to those obtained with maug-cc-pVTZ.

Previous studies[20,21,43,80] have already shown that the Minnesota functionals give reliable equilibrium geometries; however, in this work we are concerned with how well the equilibrium geometries optimized with these functionals approximate the ground state structures of the reactants and products of reactions R1a−R2b. In particular, we are interested in the deviations between the principal moments of inertia of the ground state

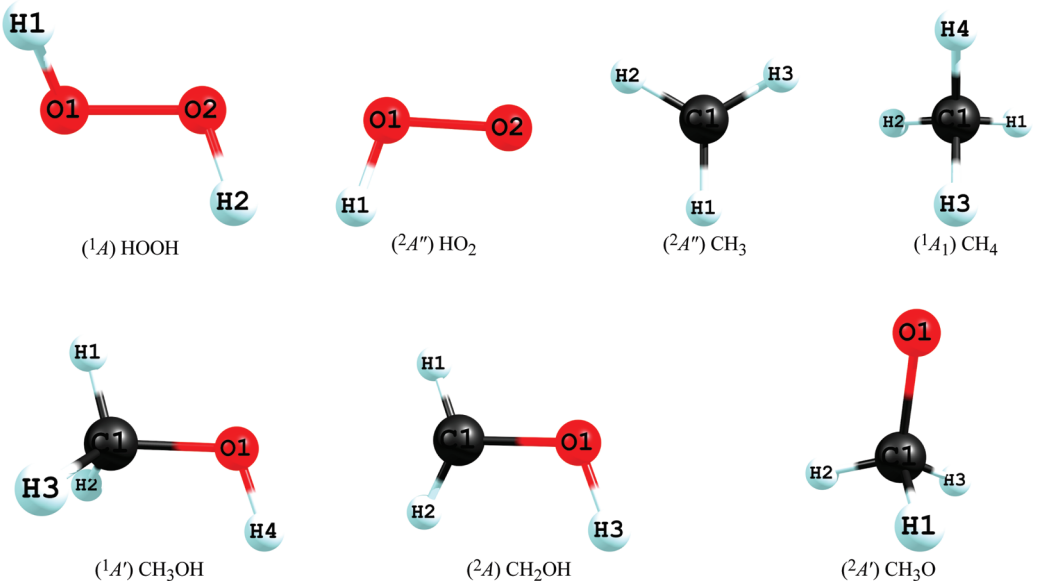

Figure 1. Reactants and products for reactions of methanol with hydroperoxyl and methyl radicals.

structures and their computed equilibrium counterparts—since these quantities are used to obtain the rotational partition functions needed to calculate rate coefficients via transition state theory. The computed products of the principal moments of inertia for all reactants and products are also listed in Table 14.

In Table 14, the experimental values for the geometric parameters and products of the moments of inertia are taken from the Computational Chemistry Comparison and Benchmark Database[19] for all species except CH_2OH and CH_3O. For the highly nonrigid CH_2OH and CH_3O radicals, we instead compare our calculated equilibrium geometries, which belong to the C_s and C_1 point groups, respectively, to their respective C_{3v} and C_s analogues from the high-level computations of Marenich and Boggs[9,10]—assumed to closely approximate the true vibrationally averaged ground state geometries—and we compare the products of the moments of inertia for the equilibrium structures we obtained to those derived from the ground state rotational constants (A_0, B_0, and C_0) Marenich and Boggs calculated from the respective ground vibronic states of CH_2OH and CH_3O.

From an inspection of Table 14, we can see that the equilibrium geometries computed with the various Minnesota functionals are all in good agreement with their experimental counterparts for ground state structures, even for the highly nonrigid CH_2OH and CH_3O radicals, yielding MUEs of 1% for bond lengths (R), 2% for bond angles (A), 3−4% for dihedral angles (D), and 4−9% for the products of the principal moments of inertia ($I_AI_BI_C$). In addition, the computed geometries and products of the principal moments of inertia are very similar for all Minnesota functionals. The choice of triple-ζ basis set does not significantly change the geometries and the products of the principal moments of inertia.

The geometries of the transition states for the four methanol reactions are depicted in Figure 2 and given in Tables 15 and 16. These transition state structures represent the lowest energy torsional conformers for all the DFT-based electronic model chemistries tested in this work. As was the case with the geometries of the reactants and products, the transition state geometries computed with the various DFT-based electronic model chemistries were very similar, and in order to avoid being redundant, we have only tabulated the geometries optimized with M06-2X/MG3S, which were used in all single-point calculations throughout this work, and those optimized with M08-HX55/maug-cc-pVTZ for TS1a and TS1b and M08-HX/maug-cc-pVTZ for TS2a and TS2b, which will be used in our dynamics study of these reactions systems. However, in the Supporting Information, we give the geometries of the four transitions states computed with all of the DFT-based electronic model chemistries employed in this work. Finally, we note that the transition state geometries we obtained for reactions R1a and R1b with the various DFT-based electronic model chemistries are in good agreement with those optimized with CASPT2/cc-pVTZ for the same reactions in recent investigations.[5,6,81]

3.3.4. Zero-Point Energies. The computed ZPEs for the reactants and products of reactions R1a−R2b are given and compared with experiment in Table 17. The DFT results presented in Table 17 correspond to scaled ZPEs, where the scale factors employed are taken from our recent compilation[15] of optimized ZPE scale factors and have values of 0.962 for M05-2X/MG3S, 0.970 for M06-2X/MG3S, 0.983 for M08-SO/MG3S, 0.973 for M08-HX/MG3S, 0.976 for M08-HX/ma-TZVP, and 0.976 for M08-HX/maug-cc-pVTZ; we derived a scale factor of 0.957 for M08-HX55/maug-cc-pVTZ in the present study based on the reduced scale factor optimization model proposed in prior work.[15]

The scaled computed ZPEs are in good accord with experiment for the electronic model chemistries examined here, with MUEs in the range of 0.24−0.38 kcal mol^{-1}. The best performance in the case of ZPEs is for M05-2X/MG3S. We note that M08-HX/maug-cc-pVTZ and M08-HX55/maug-cc-pVTZ, which we will use for the future dynamics calculations based on the performance of these electronic model chemistries for zero-point-exclusive barrier heights and reaction energies, also perform reasonably well with respect to ZPEs, with respective MUEs of 0.34 and 0.35 kcal mol^{-1}.

The scaled ZPEs of the lowest energy transition state structures for the four methanol reactions are given in Table 18. For succinctness, we once again confine our discussion to (and have

Table 14. Comparison of DFT and Experimental Geometries for Reactants and Products of Methanol Reactions

species	parameter[a]	experiment	M05-2X/ MG3S	M06-2X/ MG3S	M08-SO/ MG3S	M08-HX/ MG3S	M08-HX/ ma-TZVP	M08-HX/ maug-TZ	M08-HX55/ maug-TZ
HO_2	R(O−H)	0.971	0.969	0.972	0.976	0.969	0.971	0.969	0.962
	R(O−O)	1.331	1.307	1.306	1.303	1.303	1.302	1.305	1.294
	A(H−O−O)	104.3	105.9	106.0	106.5	106.3	106.4	106.1	106.3
	$I_AI_BI_C$	199	178	178	178	175	175	178	168
HOOH	R(O−H)	0.950	0.961	0.963	0.967	0.961	0.963	0.961	0.954
	R(O−O)	1.475	1.420	1.420	1.417	1.420	1.420	1.423	1.409
	A(H−O−O)	94.8	101.5	101.6	102.0	101.7	101.5	101.5	101.8
	D(H−O−O−H)	119.8	113.5	112.9	113.7	113.1	115.6	114.1	114.0
	$I_AI_BI_C$	646	571	574	574	571	572	576	544
CH_3[b]	R(C−H)	1.079	1.074	1.076	1.084	1.079	1.081	1.079	1.071
	$I_AI_BI_C$	11	11	11	11	11	11	11	11
CH_4[c]	R(C−H)	1.087	1.085	1.087	1.094	1.090	1.092	1.090	1.082
	$I_AI_BI_C$	33	32	32	33	33	33	33	31
CH_3O	R(C−O)	1.374	1.370	1.366	1.365	1.362	1.363	1.364	1.355
	R(C−H1)	1.094	1.099	1.103	1.112	1.107	1.108	1.107	1.098
	R(C−H2)	1.094	1.091	1.094	1.102	1.099	1.101	1.099	1.091
	A(H1−C−O)	110.3	105.0	105.3	105.0	105.5	105.5	105.5	105.6
	A(H2−C−O)	110.3	112.5	112.8	113.0	112.9	112.9	112.9	112.8
	D(H1−C−O−H2)	120.0	116.3	116.2	115.9	116.2	116.2	116.2	116.3
	$I_AI_BI_C$	1066	1044	1042	1060	1044	1049	1047	1005
CH_2OH	R(O−H3)	0.960	0.957	0.959	0.962	0.957	0.958	0.957	0.949
	R(C−O)	1.368	1.360	1.358	1.358	1.355	1.355	1.357	1.347
	R(C−H1)	1.075	1.073	1.077	1.083	1.079	1.081	1.079	1.071
	R(C−H2)	1.078	1.076	1.080	1.086	1.082	1.084	1.082	1.074
	A(H1−C−O)	115.2	114.1	113.8	114.7	114.5	114.4	114.5	114.6
	A(H2−C−O)	120.5	118.9	118.8	119.5	119.4	119.3	119.3	119.3
	A(H3−O−C)	108.3	110.2	110.2	111.0	110.7	110.5	110.4	110.6
	D(H1−C−O−H3)	180.0	175.9	174.9	176.8	176.3	176.5	176.5	176.7
	$I_AI_BI_C$	864	829	831	842	826	828	829	793
CH_3OH[d]	R(O−H4)	0.956	0.956	0.958	0.961	0.956	0.957	0.956	0.949
	R(C−O)	1.427	1.418	1.413	1.415	1.411	1.410	1.413	1.402
	R(C−H)	1.096	1.087	1.091	1.098	1.095	1.097	1.095	1.087
	A(H−C−O)	109.9	110.1	110.3	110.4	110.5	110.5	110.5	110.5
	A(H4−O−C)	108.9	109.2	109.2	109.8	109.4	109.2	109.2	109.4
	A(H−C−H)	109.0	108.9	108.6	108.5	108.4	108.4	108.4	108.4
	$I_AI_BI_C$	1724	1663	1656	1693	1663	1667	1669	1593
MUE	R	–	0.009 (1%)	0.010 (1%)	0.013 (1%)	0.011 (1%)	0.011 (1%)	0.010 (1%)	0.015 (1%)
MUE	A	–	2.1 (2%)	2.2 (2%)	2.4 (2%)	2.2 (2%)	2.2 (2%)	2.1 (2%)	2.2 (2%)
MUE	D	–	4.7 (4%)	5.2 (4%)	4.5 (3%)	4.7 (4%)	3.8 (3%)	4.3 (3%)	4.3 (3%)
MUE	$I_AI_BI_C$	–	31 (6%)	32 (5%)	22 (4%)	32 (5%)	30 (5%)	29 (5%)	58 (9%)

[a] Bond lengths are in Å, bond and dihedral angles are in degrees, and products of principal moments of inertia are in amu^3 Å^6. [b] All angles are 120.0° by definition. [c] All angles are 109.471° by definition. [d] R(CH), A(HCO), and A(HCH) represent averages over all three H-atoms in the CH_3 fragment. D(H−C−O−H) is 180.0° by definition.

only tabulated) the results for the transition states obtained with M06-2X/MG3S for all four reactions, M08-HX55/maug-cc-pVTZ for reactions R1a and R1b and M08-HX/maug-cc-pVTZ for reactions R2a and R2b. Adding the difference between the ZPEs of each transition state and the corresponding reactants to the zero-point-exclusive barrier heights yields the zero-point-inclusive barrier heights for reactions R1a−R2b, which correspond to the difference between the energy of the saddle point and that of the reactants on the vibrationally adiabatic ground state potentials for these reactions, $\Delta_f V_a^{G\ddagger}$. The same can be done for the reverse processes of reactions R1a−R2b to obtain $\Delta_r V_a^{G\ddagger}$, and we present these values for both the forward and reverse reactions in Table 19.

3.4. Best Estimates of Zero-Point-Inclusive Reaction Barrier Heights. In this section, we estimate values for the zero-point-inclusive forward and reverse barrier heights for reactions R1a−R2b. To arrive at these estimates, we add ZPE contributions to our best estimates of the zero-point-exclusive barrier heights, namely those obtained using CCSDT(2)$_Q$/CBS-(aT+aQ) + CV + R single-point energy calculations at geometries optimized with M06-2X/MG3S (Table 8).

dx.doi.org/10.1021/jp110024e |J. Phys. Chem. A 2011, 115, 2811–2829

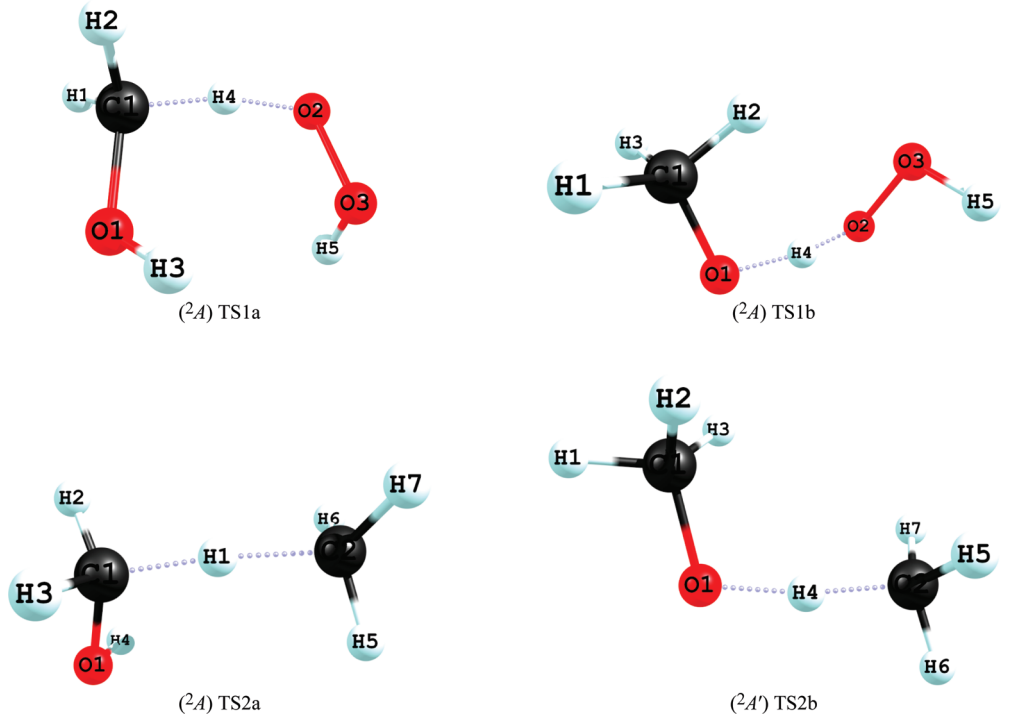

Figure 2. Transition states for reactions of methanol with hydroperoxyl and methyl radicals.

Table 15. Selected DFT Geometries for Transition States of Reactions R1a and R1b

TS1a			TS1b		
parameter[a]	M06-2X/MG3S	M08-HX55/maug-cc-pVTZ	parameter[a]	M06-2X/MG3S	M08-HX55/maug-cc-pVTZ
R(C1−O1)	1.370	1.358	*R*(C1−O1)	1.374	1.364
R(C1−H1)	1.085	1.080	*R*(C1−H1)	1.096	1.092
R(C1−H2)	1.091	1.086	*R*(C1−H2)	1.105	1.102
R(O1−H3)	0.963	0.953	*R*(C1−H3)	1.092	1.089
R(O2−O3)	1.383	1.375	*R*(O2−O3)	1.377	1.359
R(O3−H5)	0.965	0.955	*R*(O3−H5)	0.966	0.957
R(H4−O2)	1.227	1.214	*R*(O1−H4)	1.268	1.237
R(C1−H4)	1.305	1.310	*R*(H4−O2)	1.088	1.101
A(O1−C1−H1)	110.5	110.9	*A*(O1−C1−H1)	109.1	109.6
A(O1−C1−H2)	115.2	115.5	*A*(O1−C1−H2)	108.8	109.3
A(C1−O1−H3)	109.1	109.4	*A*(O1−C1−H3)	113.1	113.1
A(O1−C1−H4)	106.1	106.1	*A*(C1−O1−H4)	109.8	109.2
A(H1−C1−H2)	114.4	114.4	*A*(H1−C1−H2)	105.2	105.2
A(H1−C1−H4)	107.1	106.8	*A*(H1−C1−H3)	111.0	110.8
A(H2−C1−H4)	102.6	102.0	*A*(H2−C1−H3)	109.2	108.6
A(O2−O3−H5)	103.4	103.5	*A*(O2−O3−H5)	103.7	104.2
A(O3−O2−H4)	102.5	102.4	*A*(O3−O2−H4)	105.6	106.2
A(O2−H4−C1)	161.4	161.4	*A*(O1−H4−O2)	167.0	167.5
D(H3−O1−C1−H4)	62.5	62.1	*D*(H1−C1−O1−H4)	−140.4	−139.8
D(O1−C1−H4−O2)	−24.2	−26.1	*D*(C1−O1−H4−O2)	17.5	22.6
D(C1−H4−O2−O3)	2.6	4.3	*D*(O1−H4−O2−O3)	22.2	13.1
D(H4−O2−O3−H5)	94.1	95.5	*D*(H4−O2−O3−H5)	89.8	91.2
$I_AI_BI_C$	626 501	610 154	$I_AI_BI_C$	601 097	571 892

[a] Bond lengths are in Å, bond and dihedral angles are in degrees, and products of principal moments of inertia are in amu^3 Å^6.

Scaling the ZPEs computed with the various DFT-based electronic model chemistries in Table 17 for the reactants and products of reactions R1a−R2b resulted in anharmonic ZPEs that are in good agreement with experiment, suggesting that the

dx.doi.org/10.1021/jp110024e |J. Phys. Chem. A 2011, 115, 2811–2829

Table 16. Selected DFT Geometries for Transition States of Reactions R2a and R2b

TS2a			TS2b		
parameter[a]	M06-2X/MG3S	M08-HX/maug-cc-pVTZ	parameter[a]	M06-2X/MG3S	M08-HX/maug-cc-pVTZ
R(C1−O1)	1.389	1.389	*R*(C1−O1)	1.396	1.396
R(C1−H2)	1.091	1.096	*R*(C1−H1)	1.094	1.098
R(C1−H3)	1.086	1.090	*R*(C1−H2)	1.094	1.098
R(O1−H4)	0.959	0.957	*R*(C1−H3)	1.094	1.098
R(C2−H5)	1.084	1.086	*R*(C2−H5)	1.085	1.087
R(C2−H6)	1.084	1.087	*R*(C2−H6)	1.084	1.087
R(C2−H7)	1.084	1.086	*R*(C2−H7)	1.085	1.087
R(C1−H1)	1.286	1.294	*R*(O1−H4)	1.231	1.224
R(H1−C2)	1.420	1.419	*R*(H4−C2)	1.261	1.278
A(O1−C1−H2)	114.3	114.4	*A*(O1−C1−H1)	105.9	106.3
A(O1−C1−H3)	109.2	109.3	*A*(O1−C1−H2)	112.6	112.7
A(C1−O1−H4)	109.6	109.7	*A*(O1−C1−H3)	112.6	112.7
A(O1−C1−H1)	109.3	109.7	*A*(C1−O1−H4)	106.6	106.4
A(H2−C1−H3)	112.2	112.1	*A*(H1−C1−H2)	107.9	107.7
A(H2−C1−H1)	105.8	105.6	*A*(H1−C1−H3)	107.9	107.7
A(H3−C1−H1)	105.5	105.3	*A*(H2−C1−H3)	109.7	109.5
A(H5−C2−H6)	114.3	114.5	*A*(H5−C2−H6)	113.6	113.9
A(H5−C2−H7)	114.3	114.5	*A*(H5−C2−H7)	113.6	113.9
A(H5−C2−H1)	102.9	103.0	*A*(H5−C2−H4)	105.4	104.9
A(H6−C2−H7)	114.1	114.2	*A*(H6−C2−H7)	113.6	113.9
A(H6−C2−H1)	104.9	104.7	*A*(H6−C2−H4)	104.1	103.8
A(H7−C2−H1)	104.6	104.1	*A*(H7−C2−H4)	105.4	104.9
A(C1−H1−C2)	173.3	175.0	*A*(O1−H4−C2)	171.1	171.2
D(H4−O1−C1−H1)	−70.0	−70.7	*D*(H1−C1−O1−H4)	180.0	180.0
D(O1−C1−H1−C2)	−3.4	−6.3	*D*(C1−O1−H4−C2)	0.0	0.0
D(C1−H1−C2−H5)	−31.4	−30.6	*D*(O1−H4−C2−H5)	60.2	60.2
$I_AI_BI_C$	228 158	232 246	$I_AI_BI_C$	159 707	161 676

[a] Bond lengths are in Å, bond and dihedral angles are in degrees, and products of principal moments of inertia are in amu^3 Å^6.

Table 17. Comparison of Scaled DFT ZPEs and Experimental ZPEs (in kcal mol^{-1}) for Reactants and Products of Methanol Reactions

species	experiment	M05-2X/MG3S	M06-2X/MG3S	M08-SO/MG3S	M08-HX/MG3S	M08-HX/ma-TZVP	M08-HX/maug-cc-pVTZ	M08-HX55/maug-cc-pVTZ
HO_2	8.70 ± 0.14	8.86	8.93	8.98	9.01	9.01	9.00	9.01
HOOH	16.33 ± 0.26	16.51	16.65	16.71	16.72	16.69	16.70	16.71
CH_3	18.68 ± 0.30	18.35	18.07	18.18	18.24	18.27	18.31	18.28
CH_4	27.83 ± 0.45	27.47	27.40	27.30	27.30	27.33	27.36	27.31
CH_3O	22.60	22.63	22.49	22.30	22.31	22.36	22.40	22.40
CH_2OH	22.59 ± 0.02	22.85	22.92	22.75	22.85	22.95	22.93	22.88
CH_3OH	31.85 ± 0.51	31.53	31.53	31.50	31.41	31.50	31.52	31.48
MUE	−	0.24	0.33	0.36	0.38	0.36	0.34	0.35

scaled ZPEs computed with these electronic model chemistries for the transition states of reactions R1a−R2b should also be reliable; however, the quality of these ZPEs can be further improved through the application of scale factors customized specifically for these reactions. We optimized specific-reaction scale factors for the two electronic model chemistries of most interest (M08-HX/maug-cc-pVTZ and M08-HX55/maug-cc-pVTZ) by minimizing the root-mean-square deviations between the computed and experimental ZPEs for all of the reactants and products of reactions R1a−R2b using eq 12 from Alecu et al.[15] The specific-reaction scale factors obtained for M08-HX/maug-cc-pVTZ and M08-HX55/maug-cc-pVTZ have values of 0.981 and 0.963, respectively, which correspond to increases of just 0.005 and 0.006 from their original respective values. The anharmonic ZPEs obtained by scaling the harmonic ZPEs computed with M08-HX/maug-cc-pVTZ by 0.981 were added to the appropriate CCSDT(2)$_Q$/CBS-(aT+aQ) + CV + R//M06-2X-MG3S electronic energies to

dx.doi.org/10.1021/jp110024e |J. Phys. Chem. A 2011, 115, 2811–2829

yield our best estimates of the zero-point-inclusive barrier heights for reactions R1a−R2b given in Table 19.

As already noted in sections 3.3.1 and 3.3.2, the M08-HX55/maug-cc-pVTZ zero-point-exclusive barrier heights agree well with our best estimates for the barrier heights of reactions R1a and R1b and the M08-HX/maug-cc-pVTZ results are in good accord with the best estimates for the barrier heights of reactions R2a and R2b. Table 19 shows that the zero-point-inclusive barrier heights computed via CCSD(T)/CBS//CASPT2/cc-pVTZ for reactions R1a and R1b in recent studies by Klippenstein and coauthors[5,6] are in good agreement with our best estimates, except for $\Delta_r V_a^{G\ddagger}$ for reaction R1b, which seems to be appreciably overestimated by CCSD(T)/CBS//CASPT2/cc-pVTZ (0.88 kcal mol^{-1}). Table 19 also lists values for the computed enthalpies of reaction at 0 K (ΔH_0°) for reactions R1a−R2b, obtained as the difference of the zero-point-inclusive barrier heights. Comparisons to the experimental values for ΔH_0° in Table 3 indicate that, overall, all electronic model chemistries considered in this section perform reasonably well for ΔH_0°; in fact, the CCSD(T)/CBS//CASPT2-cc-pVTZ ΔH_0° value obtained by Klippenstein and co-workers[5,6] for reaction R1a agrees with experiment, as do the ΔH_0° values computed with M08-HX55/maug-cc-pVTZ (with a general or specific-reaction scale factor) for reactions R1a and R1b, and the ΔH_0° values computed with CCSDT(2)$_Q$/CBS(aT+aQ) + CV + R//M06-2X/MG3S for reactions R1b, R2a, and R2b.

4. SUMMARY AND RECOMMENDATIONS

We have compiled a database of accurate experimental zero-point-exclusive bond energies and reaction energies for the reactions of methanol with the hydroperoxyl and methyl radicals and found that these can be predicted reliably by a single-reference approach based on M06-2X/MG3S geometries and single-point energy calculations using coupled cluster theory with single, double, triple, and a second-order perturbative treatment of quadruple excitations extrapolated to the complete basis set limit from augmented triple- and quadruple-ζ basis sets and including core−valence and scalar relativistic effects: CCSDT(2)$_Q$/CBS(aT+aQ) + CV + R//M06-2X/MG3S. The addition of accurate barrier heights calculated with this model electronic chemistry to the aforementioned experimental bond energies and reaction energies led to the formulation of our final database against which several more affordable electronic model chemistries have been validated.

To best assess the performance of the electronic model chemistries tested, we averaged the MUEs for reaction energies and barrier heights, since these are the quantities of interest from a dynamics point of view, and we report these in Table 20. In addition, in Table 20, we estimate the relative computational cost associated with each electronic model chemistry we have considered in this work by taking the average of the total CPU times (processors times hours) required for the single-point energy calculation of each of the four transition states, and dividing this quantity by precisely the same quantity obtained from HF/cc-pVDZ single-point calculations using the same computational software and the same computer. In cases where the final results of a particular electronic model chemistry entailed the combination of individual calculations obtained with different programs, each program-specific component was compared to its HF/cc-pVDZ analogue computed on the same computer with the same program. Finally, since for most systems the choice of the size of the integration grid is not obvious a priori, we note that the cost for the DFT-based electronic model chemistries was obtained from single-point calculations that employed the default integration grid in Gaussian.

We found that when extrapolating to the CBS limit, it is not necessary to go beyond CCSD(T) theory extrapolated to the CBS limit from unaugmented cc-pVTZ and cc-pVQZ basis sets to accurately reproduce all the properties in question; i.e., the cumulative effects of basis set augmentation, full triple excitations, quadruple excitations approximated via a second-order perturbative treatment, core−valence correlation, and scalar relativity are only marginal and unnecessary for attaining benchmarking-quality results and increase the computational cost by a factor of 8 for the present systems. We also found that the explicitly correlated CCSD(T)-F12a and CCSD(T)-F12b methods accompanied by the minimally augmented triple-ζ basis set maug-cc-pVTZ can also yield results of benchmarking quality, at an even more reduced computational cost—a factor of 78 cheaper than our most expensive calculation. We recommend the use of these

Table 18. Scaled DFT ZPEs (in kcal mol^{-1}) of Transition States for the Four Methanol Reactions Considered

species	M06-2X/MG3S	M08-HX/maug-cc-pVTZ	M08-HX55/maug-cc-pVTZ
TS1a	38.99	−	39.01
TS1b	37.73	−	37.72
TS2a	48.97	49.13	−
TS2b	48.80	48.61	−

Table 19. Computed Zero-Point-Inclusive Barrier Heights and Enthalpies for Reactions R1a−R2b in kcal mol^{-1}

	forward barrier height ($\Delta_f V_a^{G\ddagger}$) (kcal mol^{-1})				reverse barrier height ($\Delta_r V_a^{G\ddagger}$) (kcal mol^{-1})				forward reaction enthalpy (ΔH_0°) (kcal mol^{-1})			
electronic model chemistry	R1a	R1b	R2a	R2b	R1a	R1b	R2a	R2b	R1a	R1b	R2a	R2b
M08-HX/maug-cc-pVTZ[a]	14.61	19.60	12.61	12.30	5.96	1.75	21.95	12.44	8.65	17.85	−9.34	−0.14
M08-HX/maug-cc-pVTZ[b]	14.60	19.59	12.61	12.30	5.96	1.74	21.95	12.43	8.64	17.85	−9.34	−0.13
M08-HX55/maug-cc-pVTZ[a]	15.47	20.88	−	−	7.11	2.88	−	−	8.36	18.00	−	−
M08-HX55/maug-cc-pVTZ[b]	15.46	20.87	−	−	7.10	2.87	−	−	8.36	18.00	−	−
CCSD(T)/CBS//CASPT2/cc-pVTZ[c]	15.27	21.24	−	−	7.01	3.56	−	−	8.26	17.68	−	−
best estimate[d]	15.40	20.81	12.93	12.58	6.72	2.68	21.57	11.77	8.68	18.13	−8.64	0.81

[a] The ZPEs used to obtain these results were scaled by general scale factors. [b] The ZPEs used to obtain these results were scaled by specific-reaction scale factors (see section 3.4). [c] Taken from refs 5 and 6. [d] CCSDT(2)$_Q$/CBS(aT+aQ) + CV + R single-point energies on M06-2X/MG3S geometries and M08-HX/maug-cc-pVTZ ZPEs scaled by a specific-reaction scale factor (0.981).

Table 20. Summary of MUEs for Thermochemical Kinetics and Relative Computational Costs for Electronic Model Chemistries

electronic model chemistry[a]	MUE[b]	cost[c]
$CCSDT(2)_Q$/CBS(aT+aQ) + CV + R	0.10	78 000
CCSD(T)/CBS(T+Q) + CV + R	0.13	15 000
CCSDT/CBS(T+Q) + CV + R	0.14	16 000
CCSD(T)/CBS(aT+aQ)	0.14	62 000
CCSD(T)-F12b/maug-cc-pVTZ	0.14	1 000
CCSD(T)/CBS(aT+aQ) + CV + R	0.15	68 000
CCSD(T)-F12b/jul-cc-pVTZ + CV + R	0.15	7 300
CCSDT/CBS(T+Q)	0.15	11 000
CCSD(T)-F12b/aug-cc-pVTZ + CV + R	0.16	10 000
CCSD(T)-F12b/jul-cc-pVTZ	0.16	2 000
CCSDT/CBS(aT+aQ)	0.16	64 000
CCSD(T)-F12a/jul-cc-pVTZ + CV + R	0.16	7 300
CCSD(T)/CBS(T+Q)	0.17	9 400
$CCSDT(2)_Q$/CBS(aT+aQ)	0.17	72 000
$CCSDT(2)_Q$/CBS(T+Q) + CV + R	0.17	25 000
CCSDT/CBS(aT+aQ) + CV + R	0.17	69 000
CCSD(T)-F12a/aug-cc-pVTZ + CV + R	0.19	10 000
CCSD(T)-F12b/aug-cc-pVTZ	0.20	4 900
CCSD(T)-F12a/jul-cc-pVTZ	0.20	2 000
CCSD(T)-F12a/maug-cc-pVTZ	0.21	1 000
$CCSDT(2)_Q$/CBS(T+Q)	0.23	19 000
CCSD(T)/maug-cc-pVTZ	0.23	980
CCSD(T)-F12a/aug-cc-pVTZ	0.24	4 900
CCSD(T)/jul-cc-pVTZ	0.32	1 600
CCSD(T)/CBS(D+T)	0.38	910
CCSD(T)/CBS(aD+aT)	0.44	3 400
MCG3-MPW	0.45	72
CCSD(T)/aug-cc-pVTZ	0.50	3 200
CCSD(T)/cc-pVTZ	0.50	860
M08-HX/maug-cc-pVTZ	0.61	43
CCSD(T)-F12b/cc-pVTZ	0.62	900
CCSD(T)-F12a/cc-pVTZ	0.65	900
BMC-CCSD	0.66	34
M08-HX/aug-cc-pVTZ	0.67	170
M08-HX/ma-TZVP	0.77	25
M08-SO/maug-cc-pVTZ	0.79	47
M08-SO/MG3S	0.79	34
M08-SO/aug-cc-pVTZ	0.81	190
CBS-QB3	0.83	230
M08-HX/MG3S	0.83	23
M08-SO/ma-TZVP	1.07	28
M05-2X/maug-cc-pVTZ	1.29	37
M05-2X/aug-cc-pVTZ	1.31	130
M05-2X/MG3S	1.45	22
M06-2X/maug-cc-pVTZ	1.47	46
M06-2X/aug-cc-pVTZ	1.50	170
M05-2X/ma-TZVP	1.51	22
M06-2X/ma-TZVP	1.55	27
M06-2X/MG3S	1.66	25
CCSD/CBS(aD+aT)	1.95	2 100
M05/MG3S	1.99	22
CCSD/CBS(D+T)	1.99	490
CCSD/CBS(T+Q)	2.15	4 200
CCSD/CBS(aT+aQ)	2.23	16 000
M06/MG3S	2.48	26

[a] Single-point calculations based on geometries optimized with M06-2X/MG3S. [b] Averaged over $V_f^{\ddagger}$, $V_r^{\ddagger}$, and ΔE values for reactions R1a−R2b (12 data). [c] Single-processor CPU time relative to equivalent HF/cc-pVDZ calculation (see section 4). For CCSD(T)-F12a and CCSD(T)-F12b, the cost given is for a single run that generates both the CCSD(T)-F12a and CCSD(T)-F12b results.

methods. In addition, we have also shown that the computational cost can be further reduced significantly (by an overall factor of ∼1100!) by using the high-performance-to-cost MCG3-MPW multicoefficient method without appreciably compromising the results, and we recommend using this method when the CCSD(T)/CBS-(T+Q) or CCSD-F12 alternatives are unaffordable or highly impractical.

Finally, we found that the M08 density functionals can achieve results for reaction energies and barrier heights of an accuracy that rivals that of CCSD(T)/aug-cc-pVTZ theory and CCSD-(T)-F12/cc-pVTZ while reducing the computational cost considerably. Not only is the cost smaller for the reactions in this paper, but the relative savings will be even greater for studies of larger molecules because of the improved scaling. We recommend the use of these Minnesota functionals in conjunction with efficient minimally augmented basis sets for kinetic applications. In particular, for the systems we have investigated, we have shown that the M08-HX density functional paired with the maug-cc-pVTZ basis set achieves the best overall performance among the DFT-based electronic model chemistries considered, and that for reactions R1a and R1b, the performance of this density functional can be further improved by slightly increasing the amount of Hartree−Fock exchange incorporated in its design to 55%. We plan to use these electronic model chemistries to study the dynamics of reactions R1a−R2b, and we recommend the use of these electronic model chemistries for the study of analogous reactions.

■ ASSOCIATED CONTENT

Supporting Information. Geometries, in Cartesian coordinates [x (Å), y (Å), z (Å)], of reactants, products, and transition states of reactions R1a−R2b optimized with the various DFT-based electronic model chemistries used in this work. This material is available free of charge via the Internet at http://pubs.acs.org.

■ AUTHOR INFORMATION

Corresponding Author
*E-mail: truhlar@umn.edu.

■ ACKNOWLEDGMENT

The authors are grateful to Yan Zhao and Rex T. Skodje for helpful assistance. This material is based on work supported as part of the Combustion Energy Frontier Research Center, funded by the U.S. Department of Energy, Office of Science, Office of Basic Energy Sciences under Award No. DE-SC

0001198. Additional support was provided by the Office of Basic Energy Sciences under Grant DE-FG02-86ER13579.

REFERENCES

(1) Norton, T. S.; Dryer, F. L. *Symp. (Int.) Combust., [Proc.]* **1990**, *23rd*, 179.
(2) Hess, W. P.; Tully, F. P. *Chem. Phys. Lett.* **1988**, *152*, 183.
(3) Norton, T. S.; Dryer, F. L. *Combust. Sci. Technol.* **1989**, *63*, 107.
(4) Norton, T. S.; Dryer, F. L. *Int. J. Chem. Kinet.* **1990**, *22*, 219.
(5) Klippenstein, S. J.; Harding, L. B.; Davis, M. J.; Tomlin, A. S.; Skodje, R. T. *Proc. Combust. Inst.* **2011**, *33*, 351.
(6) Skodje, R. T.; Tomlin, A. S.; Klippenstein, S. J.; Harding, L. B.; Davis, M. J. *J. Phys. Chem. A* **2010**, *114*, 8286.
(7) Brossard, S. D.; Carrick, P. G.; Chappell, E. L.; Hulegaard, S. C.; Engelking, P. C. *J. Chem. Phys.* **1986**, *84*, 2459.
(8) Johnson, R. D., III; Hudgens, J. W. *J. Phys. Chem.* **1996**, *100*, 19874.
(9) Marenich, A. V.; Boggs, J. E. *J. Chem. Phys.* **2003**, *119*, 3098.
(10) Marenich, A. V.; Boggs, J. E. *J. Mol. Struct.* **2006**, *780*−*781*, 163.
(11) Marenich, A. V.; Boggs, J. E. *Chem. Phys. Lett.* **2005**, *404*, 351.
(12) Marenich, A. V.; Boggs, J. E. *J. Chem. Phys.* **2005**, *122*, 024308.
(13) Marenich, A. V.; Boggs, J. E. *J. Chem. Phys.* **2003**, *119*, 10105.
(14) Pople, J. A. *Rev. Mol. Phys.* **1999**, *71*, 267.
(15) Alecu, I. M.; Zheng, J.; Zhao, Y.; Truhlar, D. G. *J. Chem. Theory Comput.* **2010**, *6*, 2872.
(16) Ruscic, B.; Pinzon, R. E.; Morton, M. L.; von Laszevski, G.; Bittner, S. J.; Nijsure, S. G.; Amin, K. A.; Minkoff, M.; Wagner, A. F. *J. Phys. Chem. A* **2004**, *108*, 9979.
(17) Ruscic, B.; Boggs, J. E.; Burcat, A.; Csaszar, A. G.; Demaison, J.; Janoschek, R.; Martin, J. M. L.; Morton, M. L.; Rossi, M. J.; Stanton, J. F.; Szalay, P. G.; Westmoreland, P. R.; Zabel, F.; Berces, T. *J. Phys. Chem. Ref. Data* **2005**, *34*, 573.
(18) Ruscic, B.; Pinzon, R. E.; Morton, M. L.; Srinivasan, N. K.; Su, M.-C.; Sutherland, J. W.; Michael, J. V. *J. Phys. Chem. A* **2006**, *110*, 6592.
(19) Johnson, R. D., III. *Computational Chemistry Comparison and Benchmark Database*, version 14; National Institute of Standards and Technology. http://cccbdb.nist.gov (accessed Aug 9, 2010).
(20) Zhao, Y.; Truhlar, D. G. *Theor. Chem. Acc.* **2008**, *120*, 215.
(21) Zhao, Y.; Truhlar, D. G. *Acc. Chem. Res.* **2008**, *41*, 157.
(22) Zheng, J.; Truhlar, D. G. *Phys. Chem. Chem. Phys.* **2010**, *12*, 7782.
(23) Purvis, G. D.; Bartlett, R. J. *J. Chem. Phys.* **1982**, *76*, 1910.
(24) Raghavachari, K.; Trucks, G. W.; Pople, J. A.; Head-Gordon, M. *Chem. Phys. Lett.* **1989**, *157*, 479.
(25) Lee, Y. S.; Kucharski, S. A.; Bartlett, R. J. *J. Chem. Phys.* **1984**, *81*, 5906.
(26) Hirata, S.; Fan, P.-D.; Auer, A. A.; Nooijen, M.; Piecuch, P. *J. Chem. Phys.* **2004**, *121*, 12197.
(27) Dunning, T. H., Jr. *J. Chem. Phys.* **1989**, *90*, 1007.
(28) Kendall, R. A.; Dunning, T. H., Jr.; Harrison, R. J. *J. Chem. Phys.* **1992**, *96*, 6796.
(29) Woon, D. E.; Dunning, T. H., Jr. *J. Chem. Phys.* **1993**, *98*, 1358.
(30) Schwenke, D. W. *J. Chem. Phys.* **2005**, *122*, 014107.
(31) Truhlar, D. G. *Chem. Phys. Lett.* **1998**, *294*, 45.
(32) Peterson, K. A.; Dunning, T. H., Jr. *J. Chem. Phys.* **2002**, *117*, 10548.
(33) Cowan, R. D.; Griffin, D. C. *J. Opt. Soc. Am.* **1976**, *66*, 1010.
(34) Adler, T. B.; Knizia, G.; Werner, H.-J. *J. Chem. Phys.* **2007**, *127*, 221106. Knizia, G.; Adler, T. B.; Werner, H.-J. *J. Chem. Phys.* **2009**, *130*, 054104.
(35) Papajak, E.; Truhlar, D. G. *J. Chem. Theory Comput.* **2010**, *6*, 597.
(36) Papajak, E.; Leverentz, H. R.; Zheng, J.; Truhlar, D. G. *J. Chem. Theory Comput.* **2009**, *5*, 1197.
(37) Montgomery, J. A., Jr.; Frisch, M. J.; Ochterski, J. W.; Petersson, G. A. *J. Chem. Phys.* **1999**, *110*, 2822.
(38) Lynch, B. J.; Zhao, Y.; Truhlar, D. G. *J. Phys. Chem. A* **2005**, *109*, 1643.
(39) Zhao, Y.; Truhlar, D. G. *J. Phys. Chem. A* **2005**, *109*, 4209.
(40) Zheng, J.; Zhao, Y.; Truhlar, D. G. *J. Chem. Theory Comput.* **2009**, *5*, 808.
(41) Zhao, Y.; Schultz, N. E.; Truhlar, D. G. *J. Chem. Phys.* **2005**, *123*, 161103.
(42) Zhao, Y.; Schultz, N. E.; Truhlar, D. G. *J. Chem. Theory Comput.* **2006**, *2*, 364.
(43) Zhao, Y.; Truhlar, D. G. *J. Chem. Theory Comput.* **2008**, *4*, 1849.
(44) Lynch, B. J.; Zhao, Y.; Truhlar, D. G. *J. Phys. Chem. A* **2003**, *107*, 1384.
(45) Weigend, F.; Haser, M.; Patzelt, H.; Ahlrichs, R. *Chem. Phys. Lett.* **1998**, *294*, 143.
(46) Weigend, F.; Ahlrichs, R. *Phys. Chem. Chem. Phys.* **2005**, *7*, 3297.
(47) Zheng, J.; Xu, X.; Truhlar, D. G. *Theor. Chem. Acc.* **2011**, *128*, 295.
(48) Werner, H.-J.; Knowles, P. J.; Lindh, R.; Manby, F. R.; Schutz, M.; Celani, P.; Korona, T.; Mitrushenkov, A.; Rauhut, G.; Adler, T. B.; Amos, R. D.; Bernhardsson, A.; Berning, A.; Cooper, D. L.; Deegan, M. J. O.; Dobbyn, A. J.; Eckert, F.; Goll, E.; Hampel, C.; Hetzer, G.; Hrenar, T.; Knizia, G.; Koppl, C.; Liu, Y.; Lloyd, A. W.; Mata, R. A.; May, A. J.; McNicholas, S. J.; Meyer, W.; Mura, M. E.; Nicklass, A.; Palmieri, P.; Pfluger, K.; Pitzer, R.; Reiher, M.; Schumann, U.; Stoll, H.; Stone, A. J.; Tarroni, R.; Thorsteinsson, T.; Wang, M.; Wolf, A. *MOLPRO*, version 2009.1, a package of ab initio programs, 2009.
(49) Bylaska, E. J.; de Jong, W. A.; Govind, N.; Kowalski, K.; Straatsma, T. P.; Valiev, M.; Wang, D.; Apra, E.; Windus, T. L.; Hammond, J.; Nichols, P.; Hirata, S.; Hackler, M. T.; Zhao, Y.; Fan, P.-D.; Harrison, R. J.; Dupuis, M.; Smith, D. M. A.; Nieplocha, J.; Tipparaju, V.; Krishnan, M.; Wu, Q.; Van Voorhis, T.; Auer, A. A.; Nooijen, M.; Brown, E.; Cisneros, G.; Fann, G. I.; Fruchtl, H.; Garza, J.; Hirao, K.; Kendall, R.; Nichols, J. A.; Tsemekhman, K.; Wolinski, K.; Anchell, J.; Bernholdt, D.; Borowski, P.; Clark, T.; Clerc, D.; Dachsel, H.; Deegan, M.; Dyall, K.; Elwood, D.; Glendening, E.; Gutowski, M.; Hess, A.; Jaffe, J.; Johnson, B.; Ju, J.; Kobayashi, R.; Kutteh, R.; Lin, Z.; Littlefield, R.; Long, X.; Meng, B.; Nakajima, T.; Niu, S.; Pollack, L.; Rosing, M.; Sandrone, G.; Stave, M.; Taylor, H.; Thomas, G.; van Lenthe, J.; Wong, A.; Zhang, Z. *NWChem: A Computational Chemistry Package for Parallel Computers*, version 5.1.1; Pacific Northwest National Laboratory: Richland, WA, USA, 2008.
(50) Frisch, M. J.; Trucks, G. W.; Schlegel, H. B.; Scuseria, G. E.; Robb, M. A.; Cheeseman, J. R.; Montgomery, J. A., Jr.; Vreven, T.; Kudin, K. N.; Burant, J. C.; Millam, J. M.; Iyengar, S. S.; Tomasi, J.; Barone, V.; Mennucci, B.; Cossi, M.; Scalmani, G.; Rega, N.; Petersson, G. A.; Nakatsuji, H.; Hada, M.; Ehara, M.; Toyota, K.; Fukuda, R.; Hasegawa, J.; Ishida, M.; Nakajima, T.; Honda, Y.; Kitao, O.; Nakai, H.; Klene, M.; Li, X.; Knox, J. E.; Hratchian, H. P.; Cross, J. B.; Bakken, V.; Adamo, C.; Jaramillo, J.; Gomperts, R.; Stratmann, R. E.; Yazyev, O.; Austin, A. J.; Cammi, R.; Pomelli, C.; Ochterski, J. W.; Ayala, P. Y.; Morokuma, K.; Voth, G. A.; Salvador, P.; Dannenberg, J. J.; Zakrzewski, V. G.; Dapprich, S.; Daniels, A. D.; Strain, M. C.; Farkas, O.; Malick, D. K.; Rabuck, A. D.; Raghavachari, K.; Foresman, J. B.; Ortiz, J. V.; Cui, Q.; Baboul, A. G.; Clifford, S.; Cioslowski, J.; Stefanov, B. B.; Liu, G.; Liashenko, A.; Piskorz, P.; Komaromi, I.; Martin, R. L.; Fox, D. J.; Keith, T.; Al-Laham, M. A.; Peng, C. Y.; Nanayakkara, A.; Challacombe, M.; Gill, P. M. W.; Johnson, B.; Chen, W.; Wong, M. W.; Gonzalez, C.; Pople, J. A. *Gaussian 03*, revision E.01; Gaussian, Inc.: Wallingford, CT, USA, 2004.
(51) Zhao, Y.; Truhlar, D. G. *MN-GFM: Minnesota Gaussian Functional Module*, version 4.1; University of Minnesota: Minneapolis, MN, USA, 2008.
(52) Zhao, Y.; Truhlar, D. G. *MLGAUSS*, version 2.0; University of Minnesota: Minneapolis, MN, USA, 2005.
(53) Lee, T. J.; Taylor, P. R. *Int. J. Quantum Chem.* **1989**, *S23*, 199.
(54) Zhao, Y.; Tishchenko, O.; Gour, J. R.; Li, W.; Lutz, J. J.; Piecuch, P.; Truhlar, D. G. *J. Phys. Chem. A* **2009**, *113*, 5786.
(55) Jayatilaka, D.; Lee, T. J. *J. Chem. Phys.* **1993**, *98*, 9734.

(56) Rienstra-Kiracofe, J. C.; Allen, W. D.; Schaefer, H. F., III. *J. Phys. Chem. A* **2000**, *104*, 9823.
(57) Peiro-Garcia, J.; Nebot-Gil, I. *ChemPhysChem.* **2003**, *4*, 843.
(58) Peiro-Garcia, J.; Nebot-Gil, I. *J. Comput. Chem.* **2003**, *24*, 1657.
(59) Martinez-Avila, M.; Peiro-Garcia, J. *Chem. Phys. Lett.* **2003**, *370*, 313.
(60) Lambert, N.; Kaltsoyannis, N.; Price, S. D.; Zabka, J.; Herman, Z. *J. Phys. Chem. A* **2006**, *110*, 2898.
(61) Miller, S. R.; Schultz, N. E.; Truhlar, D. G.; Leopold, D. G. *J. Chem. Phys.* **2009**, *130*, 024304.
(62) Schultz, N. E.; Zhao, Y.; Truhlar, D. G. *J. Phys. Chem. A* **2005**, *109*, 11127.
(63) Lee, C.; Yang, W.; Parr, R. G. *Phys. Rev. B* **1988**, *37*, 785.
(64) Becke, A. D. *Phys. Rev. A* **1988**, *38*, 3098.
(65) Adamo, C.; Barone, V. *J. Chem. Phys.* **1999**, *110*, 6158.
(66) Adamo, C.; Cossi, M.; Barone, V. *THEOCHEM* **1999**, *493*, 147.
(67) Ernzerhof, M.; Scuseria, G. E. *J. Chem. Phys.* **1999**, *110*, 5029.
(68) McMillen, D. F.; Golden, D. M. *Annu. Rev. Phys. Chem.* **1982**, *33*, 493.
(69) Bak, K. L.; Jorgensen, P.; Olsen, J.; Helgaker, T.; Gauss, J. *Chem. Phys. Lett.* **2000**, *317*, 116.
(70) Feller, D.; Dixon, D. A. *J. Chem. Phys.* **2001**, *115*, 3484.
(71) Ruden, T. A.; Helgaker, T.; Jorgensen, P.; Olsen, J. *Chem. Phys. Lett.* **2003**, *371*, 62.
(72) Boese, A. D.; Oren, M.; Atasoylu, O.; Martin, J. M. L.; Kallay, M.; Gauss, J. *J. Chem. Phys.* **2004**, *120*, 4129.
(73) Ruden, T. A.; Helgaker, T.; Jorgensen, P.; Olsen, J. *J. Chem. Phys.* **2004**, *121*, 5874.
(74) Feller, D.; Peterson, K. A.; Crawford, T. D. *J. Chem. Phys.* **2006**, *124*, 54107.
(75) Karton, A.; Rabinovich, E.; Martin, J. M. L.; Ruscic, B. *J. Chem. Phys.* **2006**, *125*, 144108.
(76) Ellingson, B. A.; Theis, D. P.; Tishchenko, O.; Zheng, J.; Truhlar, D. G. *J. Phys. Chem. A* **2007**, *111*, 13554.
(77) Pu, J.; Truhlar, D. G. *J. Chem. Phys.* **2002**, *116*, 1468.
(78) Truhlar, D. G.; Wyatt, R. E. *Adv. Chem. Phys.* **1977**, *36*, 141.
(79) Dunning, T. H., Jr.; Harding, L. B. In *Theory of Chemical Reaction Dynamics*; Baer, M., Ed.; CRC Press: Boca Raton, FL, USA, 1985; Vol. 1; p 1.
(80) Zhao, Y.; Truhlar, D. G. *J. Chem. Phys.* **2008**, *128*, 184109.
(81) Skodje, R. T. University of Colorado, personal communication, 2010.